The manganese and iron shuttle in a modern euxinic basin and implications for molybdenum cycling at euxinic ocean margins

Florian Scholz*[1], James McManus[1] and Stefan Sommer[2]

[1]College of Earth, Ocean, and Atmospheric Sciences (CEOAS), Oregon State University, 104 CEOAS Administration Building, Corvallis, OR 97331-5503, USA

[2]GEOMAR Helmholtz Centre for Ocean Research Kiel, Wischhofstraße 1-3, 24148 Kiel, Germany

*Corresponding author: Phone: +1 541 737 5224, E-mail: fscholz@coas.oregonstate.edu

Resubmitted to Chemical Geology, July 3, 2013

Abstract

A meaningful application of Mo as a paleo-redox proxy requires an understanding of Mo cycling in modern reducing environments. Stagnant euxinic basins such as the Black Sea are generally regarded as model systems for understanding euxinic systems during early Earth history. However, drawing direct parallels between the Black Sea and open-marine euxinic margins is somewhat complicated by differences in the seawater residence time between these two environments. We report sediment and pore water Mo, U, Mn and Fe data for a euxinic basin with a short seawater residence time; the weakly restricted Gotland Deep in the Baltic Sea. Here, prolonged periods of euxinia alternate with brief inflow events during which well-oxygenated, saline water penetrates into the basin. During these inflow events, dissolved Mn and Fe that has accumulated within the euxinic deep water can be oxidized and precipitated. Co-variations of Mo and U within the sediment suggest that these inflow and oxygenation events may favor Mo accumulation in the sediment through adsorption to freshly oxidized Mn and Fe

21 solid phases. Once Mo is sequestered within the deeper euxinic water and sediments, Mo retention can
22 be further facilitated by conversion to thiomolybdate species and interactions with organic matter and
23 metal sulfides. By comparing our data with those from previous studies where a Mn and Fe "shuttle" for
24 Mo has been demonstrated, we identify two prerequisites for the occurrence of this mechanism. First,
25 there must be a water column oxic-anoxic redox-boundary; this provides a solubility contrast for Mn and
26 Fe. Second, the residence time of seawater in the system has to be short (weeks to a few years). The
27 latter criterion can be met through regular inflow in weakly restricted basins or upwelling in oxygen
28 minimum zones at open-marine continental margins. Based on prior work, we suggest that similar
29 conditions to those currently represented by the Gotland Deep may have prevailed at euxinic ocean
30 margins during the Proterozoic. A boundary between euxinic and oxic water masses overlying the
31 continental shelf may have resulted in accelerated Mo transport through the water column with Mn and
32 Fe (oxyhydr)oxides. We propose that this mechanism, along with Mo isotope fractionation during
33 adsorption, could contribute to the light Mo isotope composition observed in open-marine euxinic
34 sediment facies of the Proterozoic.

35 **Keywords:** Molybdenum, manganese, iron, shuttle, paleo-redox, Baltic Sea.

36 **1. Introduction**

37 The bulk concentration and isotope composition of Mo in sediments or sedimentary rocks are
38 commonly used proxies for characterizing the redox state of ancient marine systems. Their applications
39 range from the detection of reducing conditions in the bottom water or sediment pore water (e.g.,
40 Zheng et al., 2000; McManus et al., 2006; Cartapanis et al., 2011) to the identification of sulfidic
41 conditions within the water column (typically referred to as euxinia) on a global scale (Arnold et al.,
42 2004; Scott et al, 2008; Kendall et al., 2009; Dahl et al., 2011). The ability of Mo to serve as a redox
43 indicator is related to its contrasting behavior under oxic or non-sulfidic versus sulfidic conditions. In

well oxygenated waters, like those prevailing throughout most of the contemporary ocean, Mo is present as molybdate (MoO_4^{2-}). Because Mo behaves conservatively under oxic conditions, its seawater concentration (~115 nM at S = 35) and oceanic residence time (~800 ka; Bruland, 1983) are high compared to other transition metals. In the presence of dissolved sulfide, MoO_4^{2-} is converted to thiomolybdate ($MoO_xS_{4-x}^{2-}$, $1 < x < 4$) (Helz et al., 1996; Erickson and Helz, 2000). Beyond a threshold H_2S_{aq} activity ($[H_2S]_{aq}$) of approximately 11 µM (at typical seawater pH) and provided that enough time is available to attain thermodynamic equilibrium, sulfidation may be complete (Helz et al., 1996). Owing to the proclivity of thiomolybdate species for reactive surfaces, Mo is readily scavenged from sulfidic waters by forming bonds to Fe sulfides and sulfur-rich organic molecules (Emerson and Huested, 1991; Huerta-Diaz and Morse, 1992; Zheng et al., 2000; Vorlicek and Helz, 2002; Bostick et al., 2003; Tribovillard et al., 2004; Vorlicek et al., 2004; Poulson Brucker et al., 2012). As a consequence of Mo removal under sulfidic conditions, the water column in isolated euxinic basins is often depleted in Mo relative to its salinity-normalized concentration (Algeo and Lyons, 2006; Nägler et al., 2011). In a recent study, Helz et al. (2011) expanded the above concept of Mo removal from sulfidic water by emphasizing the role of pH in controlling the solubility of a nanoparticulate Fe-Mo-S mineral. According to this revised model, Mo concentrations in the water column reach a constant value once equilibrium with this nanoparticulate Fe-Mo-S mineral is attained (Helz et al., 2011).

The Mo isotope composition of modern seawater ($\delta^{98}Mo \approx 2.3$ ‰) is predominantly controlled by the input flux through river discharge and an isotopically light oxic sink associated with Mn-rich deposits in the deep-sea ($\delta^{98}Mo \approx -0.5$ ‰) (Barling et al., 2001; Siebert et al., 2003). Under persistently euxinic conditions, like those in the Black Sea below 400 m water depth, the sediment records the Mo isotope composition of seawater because Mo is quantitatively converted to MoS_4^{2-} and largely removed without fractionation from the dissolved phase (Arnold et al., 2004; Neubert et al, 2008). By analogy, if large parts of the ocean remained euxinic for a prolonged period of time (theoretically implying a global Mo

drawdown without isotope fractionation) the isotope composition of seawater would reach a new steady state value that lies closer to the isotope value of the Mo input flux from rivers. Following this concept and assuming removal of Mo into the sediments without isotope fractionation, δ^{98}Mo values intermediate between seawater and river input in euxinic sediment facies of the Proterozoic have been interpreted as an indicator for more extended euxinia during this interval of Earth history (Arnold et al., 2004; Archer and Vance, 2008; Kendall et al., 2009; Dahl et al., 2011).

The reliability of Mo isotopes as a proxy for the extent of euxinia on a global scale is dependent upon two alternative fractionation mechanisms. If $[H_2S]_{aq}$ does not reach the threshold value required for complete sulfidation of molybdate (e.g., in weakly or intermittently euxinic basins), intermediate thiomolybdate species (i.e., $MoO_3S_1^{2}$, $MoO_2S_2^{2-}$, $MoO_1S_3^{2-}$) may fractionate towards lighter values compared to the isotope composition of seawater (Tossel et al., 2005; Dahl et al., 2010; Nägler et al., 2011). Partial scavenging of intermediate thiomolybdate thus produces sedimentary δ^{98}Mo values intermediate between riverine input and contemporary seawater. An alternative mechanism for Mo removal is related to the affinity of molybdate for particulate Mn and Fe (oxyhydr)oxides. Laboratory experiments and field studies have both demonstrated that Mo adsorption to Mn and Fe (oxyhydr)oxides results in an isotope fractionation ($\Delta^{98}Mo_{seawater\text{-}adsorbed}$) of +2.8 ‰ for Mn (Siebert et al., 2003; Barling and Anbar, 2004; Wasylenki et al., 2008; Poulson Brucker et al., 2009) and +1.0 to +2.6 ‰ for Fe (Goldberg et al., 2009, 2012). Precipitation of Mn and Fe (oxyhydr)oxides at the interface between euxinic and oxic water masses may scavenge Mo that is then shuttled into the deep water or to the sediment surface (Berrang and Grill, 1974; Dellwig et al., 2010). Even though the final burial phase in the sediments after reductive re-dissolution of Mn and Fe might be similar to that of permanently euxinic basins, the Mn and Fe shuttle could potentially alter the Mo isotope composition of the deep water and sediment. Indeed, a number of studies have recognized that such a Mn and Fe shuttle enhances Mo accumulation in weakly restricted, euxinic basins (Algeo and Lyons, 2006; Algeo and Tribovillard, 2009).

92 However, its quantitative contribution to the Mo burial flux and influence on the Mo isotope
93 composition of the sediments has yet to be developed. Moreover, the actual transfer mechanism from
94 the metastable Mn or Fe (oxyhydr)oxide carrier to the final Mo burial phase has not been addressed.

95 The two removal mechanisms outlined above are particularly important where water masses with
96 contrasting redox conditions and spatially variable boundaries co-exist. Modern examples for this kind
97 of environment are intermittently euxinic basins (e.g., Cariaco Basin, Saanich Inlet; Algeo and
98 Tribovillard, 2009) or sediments underlying open-marine oxygen minimum zones at continental margins
99 (e.g., off California and Peru; Zheng et al., 2000; Scholz et al., 2011). In these environments, dynamic
100 redox interfaces between oxic and anoxic or euxinic conditions favor intense Mn and Fe redox cycling
101 with potentially important implications for the vertical transport of Mo through the water column and
102 its burial within the sediment. This same Mo shuttling could have operated in ancient oceans. For
103 instance, a number of recent studies presented evidence for localized euxinic conditions at continental
104 margins in the late Archean (Reinhard et al, 2009; Kendall et al., 2010) and the Proterozoic (e.g., Poulton
105 et al., 2010; Li et al., 2010; Johnston et al., 2010; Poulton and Canfield, 2011).

106 The Gotland Deep in the Baltic Sea is a prime locality for investigating the behavior of Mo in a dynamic
107 redox environment where both euxinic conditions and intense Mn and Fe redox cycling favor Mo
108 accumulation in the sediment. Here, extended periods of euxinia are interrupted by inflow events during
109 which saline and well-oxygenated water from the North Sea penetrates the basin (Matthäus et al.,
110 2008). These inflow and oxygenation events are accompanied by a pulsed deposition of Mn
111 (oxyhydr)oxides at the basin floor (Huckriede and Meischner, 1996; Neumann et al., 1997). In the
112 present article, we combine new pore water and sediment data for Mo and ancillary parameters with
113 data from previous studies to evaluate (1) the mechanism of Mo transfer from the water column to the
114 sediment surface and into the final burial phase (2) how the frequency of inflow events impact Mo

burial and (3) how the Mn and Fe shuttle might affect the Mo isotope composition of sediments in dynamic euxinic environments.

2. Study area

The Baltic Sea (Fig. 1A) is one of the ocean's largest brackish water basins. The estuarine circulation pattern and semi-enclosed character of the Baltic Sea promote vertical stratification and oxygen depletion below the pycnocline (Zillén et al., 2008). Owing to the characteristic seafloor topography of the Baltic Sea, euxinic conditions are largely limited to a number of sub-basins (so-called "Deeps") among which the Gotland Deep is the largest by area (Fig. 1B). The Gotland Deep has an aerial extent of ~4600 km^2 below the 150 m isobath and a maximum water depth of ~250 m (Seifert et al., 2001). The intensity and aerial extent of anoxia in the Baltic Sea has progressively increased since the industrial revolution (Zillén et al., 2008; Conley et al., 2009). This trend is generally attributed to large-scale changes in land use and eutrophication.

The water column redox structure of the Gotland Deep is affected by occasional inflow events of saline and well-oxygenated water from the North Sea. During such "Major Baltic Inflows" (MBI; Matthäus und Franck, 1992; Matthäus et al., 2008), North Sea water penetrates the Baltic Sea through the Danish Straits and, depending on the pre-existing density stratification, progressively propagates into the more distal Baltic Deeps (Fig. 1C) (Matthäus et al., 2008). After the Gotland Deep has been flushed with saline and well-oxygenated water, the deep water remains oxic for a period of several months before anoxia and eventually euxinia re-establishes (Matthäus et al., 2008). The occurrence, intensity and velocity of inflow events chiefly depend on the balance between the favoring effect of westerly winds and the impeding effect of freshwater runoff from the Baltic Sea drainage area (Schinke and Matthäus, 1998). In the long-term, both of these factors are controlled by the mean climate mode over the North Atlantic, i.e., the North Atlantic Oscillation (NAO). The NAO index is defined by the variability of the longitudinal

pressure gradient across the North Atlantic, which exerts first-order control on the intensity of westerly winds and the rainfall pattern over Northern Europe (Hurrell, 1995; Hurrell and Van Loon, 1997). Through the late 1970s, MBIs occurred frequently, either as single events (e.g., 1960, 1965; Fig. 1D) or groups of events (e.g., 1931-1938, 1948-1956, 1968-1978; Fig. 1D) (Matthäus and Franck, 1992; Matthäus et al., 2008). Since then, only a few isolated events (chiefly 1993 and 2003) have been observed, which is attributed to a shift from negative to predominantly positive NAO conditions (Hanninen et al., 2001). It has been proposed that some of the recent NAO trend is related to anthropogenic climate forcing (Visbeck et al., 2001). This relationship would link the deep water salinity and redox evolution in the Baltic Sea to global climate change.

3. Methods

Sediment and water samples were collected during Cruise AL355 of RV Alkor in May and June 2010. The water column was sampled using a CTD equipped with Niskin bottles. Short sediment cores were taken with a multiple coring device (MUC) equipped with PVC liners (inner diameter of 10 cm) (Table 1). Only sediment cores with an undisturbed sediment-water interface and at least 10 cm of bottom water overlying the sediment surface were accepted for pore water recovery. After core recovery, core liners were capped and transferred into a cooled lab container that was kept at ~6 °C. The bottom water was siphoned with a plastic tube and then filtered through cellulose acetate syringe filters. Pore water samples were obtained from parallel cores by two different methods. One core was sliced into 1 to 5 cm thick disks and the pore water was extracted with a sediment squeezer, which was operated with argon gas at pressures up to 2.5 bar. Upon squeezing, pore waters were filtered through 0.2 µm cellulose acetate membrane filters. The pore water samples obtained by this method were used for the analysis of dissolved chloride (Cl^-), sulfate (SO_4^{2-}) and total sulfide (TH_2S). A subsample of each sediment slice was stored in air-tight and pre-weighed polyethylene cups for determination of porosity as well as for acid digestions and elemental analysis after the cruise. The pore water of a second core was recovered with

Rhizons (obtained from Rhizosphere Research Products, Netherlands). To remove any oxygen prior to deployment, rhizons were preconditioned in an oxygen-free water bath. The pore water samples obtained by this technique were used for the analysis of redox-sensitive metals (Mn, Fe, Mo and U). Sub-aliquots for metal analysis were stored in acid-cleaned low-density polyethylene vials and acidified with concentrated HNO_3 (suprapur).

Analyses of dissolved oxygen (water column) and H_2S (water column, bottom and pore water) were performed onboard shortly after sample recovery. Oxygen concentrations were determined by Winkler titration and total H_2S_{aq} ($TH_2S=H_2S+HS^-+S^{2-}$) was analyzed photometrically by applying the methylene blue method (Grasshoff et al., 2002). Concentrations of Cl^- and SO_4^{2-} were measured at GEOMAR by ion chromatography (METROHM 761 Compact). Pore water salinity was calculated from Cl^- assuming a conservative Cl^- concentration of 560 mM at S = 35. Concentrations of Mn and Fe in pore water were analyzed at GEOMAR by inductively coupled plasma optical emission spectrometry (ICP-OES, VARIAN 720-ES). Samples with Mn or Fe concentrations below the detection limit of the ICP-OES method (~5 µM for Fe and ~1 µM for Mn) were analyzed by inductively coupled plasma mass spectrometry (ICP-MS) at Oregon State University (see below). The total carbon (TC), total organic carbon (TOC) and total sulfur (TS) content of freeze-dried and ground sediment samples was determined at GEOMAR using a Carlo Erba Element Analyzer (NA1500). Carbon bound to carbonates was removed by adding 1 M HCl prior to TOC analysis and total inorganic carbon (TIC) was calculated by subtracting TOC from TC. A detailed description of the above procedures may be found on the following web page: http://www.geomar.de/en/research/fb2/fb2-mg/benthic-biogeochemistry/mg-analytik/.

All of the following chemical analyses were performed at Oregon State University. Pore water samples with low concentrations of Mn and Fe were analyzed by ICP-MS (THERMO X-Series 2). A collision cell was used to minimize polyatomic interferences. Calibration standards were prepared in metal-free seawater and cobalt was used as an internal standard for mass bias correction. The Fe concentration in

common seawater standards (e.g., NASS-5; National Research Council Canada) is below the detection limit of our method. To check the reproducibility of the pore water Fe and Mn analyses, artificial pore water standards were prepared by spiking trace metal-clean seawater with an appropriate amount of Mn and Fe. Repeated analysis of samples and the artificial pore water standard (3 µM Mn and Fe) yielded a reproducibility of 1 % for both Mn and Fe. Pore water Mo and U concentrations were determined by isotope dilution (ID) ICP-MS. The Mo and U concentrations obtained for the seawater standard NASS-5 (National Research Council Canada) were 94.4±0.8 nM (n=4) (certified Mo concentration: 100 ± 10 nM) and 11.6 ± 0.1 (information value for U concentration: 10.9 nM). Major and trace elements in sediments were determined after microwave-assisted digestion in an acid mix consisting of HF, HCl and HNO_3 (Muratli et al., 2012). Certified Reference Materials (SDO-1: Devonian Ohio Shale, USGS; PACS-2: Marine Sediment, National Research Council Canada), an in-house standard (RR9702A-42MC: Chilean margin sediment), sample duplicates and method blanks were run on a regular basis to monitor the reproducibility and accuracy of the digestion procedure. Concentrations of Al, Ca, Mn and Fe in digestion solutions were determined by ICP-OES (Teledyne Leeman Prodigy). Mo and U analyses were done by ICP-MS (THERMO X-Series 2) using rhodium as an internal standard. Isotope dilution was used to verify the Mo concentrations of external standards. The reproducibility and precision of the digestion method is summarized in Table 2.

To account for dilution with detrital material, solid phase concentrations of Mn, Fe, Mo and U are reported as metal to Al or metal to TOC ratios (10^2 wt.% wt.%$^{-1}$ for Mn, wt.% wt.%$^{-1}$ for Fe, 10^4 wt.% wt.%$^{-1}$ for Mo and U). Excess metal concentrations $(Me)_{XS}$ and metal enrichment factors (ME_{EF}) are both reported with respect to the detrital background and were calculated as follows (subscripts: T=total, detr=detrital):

$$(\mathrm{Me})_{\mathrm{XS}} = (\mathrm{Me})_{\mathrm{T}} - \left(\frac{\mathrm{Me}}{\mathrm{Al}}\right)_{\mathrm{detr}} \cdot (\mathrm{Al})_{\mathrm{T}} \quad (1)$$

209 $$Me_{EF} = \frac{\left(\frac{Me}{Al}\right)_T}{\left(\frac{Me}{Al}\right)_{detr}} \quad (2)$$

210 The upper continental crust, as defined by McLennan (2001), was chosen as the detrital background
211 ($(Mo/Al)_{detr}$ = 0.19, $(U/Al)_{detr}$ = 0.35)). The Mo burial flux (F_{burial}, in nmol m^{-2} yr^{-1}) was calculated by
212 multiplying the sediment mass accumulation rate (MAR, in g m^{-2} yr^{-1}) by $(Mo)_{XS}$ (in nmol g^{-1}).

213 Concentrations and activities of aqueous species, ionic strength and saturation indexes for amorphous
214 iron monosulfide were calculated using the geochemical model PHREEQC by Parkhurst and Appelo
215 (1999). Equilibrium constants and solubility products were taken from the built-in WATEQ4F database
216 and water column pH data were taken from Ulfsbo et al. (2011). These authors measured a near-
217 constant pH of 7.3 in the deep water of the Gotland Deep (i.e., below the halocline) over a period of one
218 year during both euxinic and anoxic but non-sulfidic periods.

219 **4. Results**

220 During our sampling campaign in 2010, the salinity in the Gotland Deep water column was roughly
221 constant in the upper 50 m (S≈7) and transitioned below this to near-constant values below 150 m
222 (S≈12.5) (Fig. 2A). Oxygen was present to roughly 100 m and dissolved sulfide was detected below 120
223 m (Fig. 2B, C). The boundary between non-sulfidic and sulfidic waters is hereafter referred to as the
224 chemocline. Thermodynamic equilibrium calculations using PHREEQC reveal that the threshold activity
225 necessary for complete sulfidation of molybdate was reached below about 150 m water depth. The
226 density stratification and redox structure found in this study are in good agreement with those reported
227 in previous studies for euxinic periods in the Gotland Deep (Neretin et al, 2003; Dellwig et al, 2010;
228 Ulfsbo et al., 2011; Meyer et al., 2012)).

We present data from five cores that were retrieved along a depth transect between 65 and 223 m (Fig. 1B and Table 1). Three of these sediment cores were located above the chemocline and the remaining two sediment cores were located below the chemocline. Pore water data were obtained for the upper 15 cm for Cl^-, SO_4^{2-} and TH_2S and 9 cm for Mn, Fe, Mo and U (Fig. 3; see Electronic Supplement Table 1 for all pore water data). Pore water salinity generally increases with increasing water depth. The shallowest core (MUC02, 65 m) is the only one where SO_4^{2-} concentrations are not depleted. The remaining cores show downcore decreasing SO_4^{2-} concentrations. Concentrations of TH_2S increase in the order MUC02 ($TH_2S \leq 15$ µM) < MUC01 < MUC04 < MUC11 ≈ MUC05 ($TH_2S \leq 838$ µM), i.e., there is no clear relationship between pore water H_2S and water depth. Pore water Mn shows a transient peak in cores above the chemocline and steadily increasing concentrations with depth in cores below the chemocline. Relatively high concentrations of dissolved Fe are observed in pore waters of the shallowest core (≤107 µM) whereas the deeper cores display dissolved Fe concentrations <3 µM. Above the chemocline and below a sediment depth of 1 - 3 cm, pore waters are depleted in Mo and U with respect to their conservative values. In the shallowest core Mn, Fe and Mo display increasing concentrations below 5 cm sediment depth. Below the chemocline, pore waters are generally less depleted in Mo and U and some samples are enriched in Mo and U with respect to salinity.

Sediments above the chemocline are depleted in Mn whereas sediments below the chemocline are generally enriched in Mn with respect to the detrital background (Fig. 4; see Electronic Supplement Table 2 for all solid phase data). Cores below the chemocline display major and coincident peaks of Mn/Al (Mn ≤ 7.6 wt.%) and TIC. Ratios of Fe/Al (Fe ≤ 6.9 wt.%), Mo/Al (Mo ≤ 216 µg g^{-1}), U/Al (U ≤ 32.5 µg g^{-1}) and Mo/TOC generally increase with increasing water depth. Maxima of Fe/Al and TS occur at approximately the same sediment depth as the Mn/Al and TIC peaks. The downcore profiles of Mo/Al and U/Al are different from those of Fe/Al and TS but closely follow the depth distribution of TOC. Profiles of Mo/TOC resemble those of Mo/Al.

5. Discussion

5.1. Redox-controlled manganese and iron shuttle

The enrichments of Mn and Fe in sub-chemocline sediments of the Gotland Deep (MUC04 and MUC05) (Fig. 4) are consistent with a net transfer of detrital and diagenetically derived Mn and Fe into the euxinic basin, a so-called shuttle mechanism (e.g., Raiswell and Andersen, 2005; Lyons and Severmann, 2006; Fehr et al., 2010; Jilbert and Slomp, 2013). Sediments above the chemocline are generally depleted in Mn with respect to the detrital background, suggesting that shallower sediments are a net Mn source to the deeper basin. By contrast, the shallowest core at 65 m is the only one that is at least partly depleted in Fe and whose pore water Fe profile indicates a diffusive efflux into the water column (Fig. 3). The other cores from above the chemocline reveal pore water Fe concentrations near zero and Fe/Al ratios similar to or slightly higher than the detrital background. These observations indicate that the boundary between Fe sources and sinks is located at shallower water depths compared to that of Mn. The higher escape efficiency of Mn compared to Fe is typically observed in aquatic systems because of its higher solubility in sulfidic and slower oxidation kinetics in oxic water (e.g., Froelich et al., 1979; Canfield et al., 1993; Scholz and Neumann et al., 2007).

Sediments below the chemocline are generally enriched in Mn and Fe. However, downcore variations in Mn/Al and Fe/Al (Fig. 4) suggest that the delivery of Mn and Fe to the basin floor is not temporally uniform. The pronounced peaks of Mn/Al and inorganic carbon are a well-known phenomenon in the Baltic Deeps and their occurrence has been attributed to inflow and oxygenation events (Suess, 1979; Huckriede and Meischner, 1996; Neumann et al., 1997). Most of the Mn that enters the Gotland Deep is reductively dissolved while transiting the euxinic water column (Neretin et al., 2003; Dellwig et al., 2010). This process allows dissolved Mn to accumulate in the deep water during stagnant periods. During (oxic) inflow events, much of this Mn is re-oxidized and deposited at the basin floor. As anoxia

276 reestablishes, dissolved Mn and bicarbonate accumulate in the sediment pore water, thus promoting
277 precipitation of Ca-rich rhodochrosite ($MnCO_3$) (Huckriede and Meischner, 1996; Sternbeck and
278 Sohlenius, 1997; Neumann et al., 2002). The linear Mn-Ca relationship observed in sub-chemocline cores
279 (Fig. 5) suggests that most of the conversion of Mn (oxyhydr)oxide to rhodochrosite takes place at or
280 close to the sediment surface. However, the shallower two Mn peaks in sub-chemocline cores (8.5 cm in
281 MUC05 and 7.5 cm in MUC05) plot above the general Mn-Ca relationship. This observation could
282 indicate that a fraction of the Mn (oxyhydr)oxides does not form rhodochrosite at the sediment surface.
283 Moreover, earlier studies have demonstrated that Ca-rich rhodochrosite is metastable and undergoes
284 re-crystallization during burial (Jakobsen and Postma, 1989; Sternbeck and Sohlenius, 1997; Jilbert and
285 Slomp, 2013). This notion is consistent with the linear pore water Mn gradient in sediments below the
286 chemocline (Fig. 3). The deep-sourced Mn flux implied by this gradient could mask any shallower Mn
287 dissolution.

288 Previous studies assigned Fe enrichments in sediments of the Gotland Deep to syngenetic pyrite
289 formation in the euxinic water column (Boesen and Postma, 1988; Sternbeck and Sohlenius, 1997; Fehr
290 et al., 2010). This scenario is supported by the general co-variation between Fe/Al and TS in sub-
291 chemocline cores (Fig. 4). However, we suspect that syngenetic pyrite formation during euxinic periods
292 is unlikely to be the only mode of Fe delivery to Gotland Deep sediments. Coincident excursions of Fe/Al
293 and Mn/Al suggest that delivery of both elements is intensified during oxygenation events. Because Fe is
294 poorly soluble in both oxic and sulfidic waters, the sediments will more effectively trap Fe relative to Mn
295 and the difference between solid phase Fe maxima and minima can be less pronounced compared to
296 that of Mn. Nonetheless, the solubility of Fe in sulfidic water is about three orders of magnitude higher
297 than in oxic water (Saito et al., 2003), which is why dissolved Fe accumulates in the Gotland Deep water
298 during euxinic periods (1 - 2 µM in 2010; Meyer et al., 2012; Pohl and Fernández-Otero, 2012). Oxidation
299 and precipitation of this dissolved Fe pool during inflow events is a logical explanation for the coinciding

Fe and Mn peaks in the sediments. In contrast to Mn, Fe does not form abundant sedimentary carbonates but rather sulfide minerals in anoxic-sulfidic environments (Suess, 1979; Burdige, 1993; Sternbeck and Sohlenius, 1997). In agreement with this general observation, the coupling between Fe/Al and TS (Fig. 4) suggests that Fe sulfides represent the primary burial phase for Fe after re-dissolution of (oxyhydr)oxides. The Fe peaks at the deepest site (MUC05) are located at slightly shallower depth than the corresponding Mn peaks (Fig. 4). This observation could be explained by a shift in the ratio between marginal source to basin sink area after inflow and oxygenation events (Raiswell and Andersen, 2005). Consistent with such a scenario, Jilbert and Slomp (2013) noted accelerated accumulation of authigenic phosphorous in the deepest part of the Baltic Deeps during times of spatially more limited anoxia throughout the Holocene. Repeated dissolution and re-precipitation of Fe(oxyhydr)oxides prior to burial and conversion to Fe sulfides may further contribute to the broadening and upward shift of the Fe peaks relative to the Mn peaks.

5.2. Age constraints from the manganese and carbon record

To obtain and approximate age model and sediment mass accumulation rate within the basin we utilize the vertical succession and previously defined timing of Mn- and TIC-rich layers in the deepest core (MUC05) (Neumann et al., 1997). These authors identified three major rhodochrosite layers in the topmost 20 cm of a sediment core from 243 m water depth in the Gotland Deep. ^{210}Pb and ^{137}Cs dating suggest that these layers are a result of the inflow periods of 1931-1939, 1948-1956 and 1968-1978 (Fig. 1D; Neumann et al., 1997). The Mn and TIC peaks at 6-8 cm in MUC05 likely correspond to the last one of these extended inflow periods. Because of compaction and the comparably low sample resolution below 10 cm sediment depth, we suspect that the rhodochrosite layers corresponding to the earlier two inflow periods (Fig. 1D) are merged in MUC05. As erosion and re-dissolution prior to final burial impede the preservation of rhodochrosite layers after single and short-lived inflow events (Heiser et al., 2001), the small Mn and TIC peaks close to the sediment surface of MUC05 (1.5 cm sediment depth) could be

related to the inflow events of 1993 or 2003. Additional age information for MUC05 is obtained by comparing its TOC profile (Fig. 4) with those reported in earlier studies (Hille et al., 2006). Organic carbon accumulation in the Gotland Deep has increased from about 4 to 10 wt.% since 1900 (Hille et al, 2006). This TOC increase is located above 20 cm sediment depth in MUC05. Considering the high porosity (>0.9) and low dry bulk density (<0.5 g cm^{-3}; Leipe et al., 2011) of surface sediments in the Gotland Deep, the sediment MAR resulting from this age estimate is in good agreement with the average MAR reported for the Gotland Deep (129 ± 112 g m^{-2} yr^{-1} below 150 m water depth; Hille et al., 2006).

5.3. Controls on molybdenum accumulation

Given the well-established connection between the delivery of particulate Mn, Fe and Mo to marine sediments (Berrang and Grill, 1974; Shimmied and Price, 1986; Shaw et al., 1990; Morford et al., 2005; Scholz et al., 2011; Goldberg et al., 2012), it may be anticipated that the Mn and Fe shuttle operating in the Gotland Deep enhances the burial flux of Mo as well. Such interaction between Mn, Fe and Mo cycling has been demonstrated in other weakly restricted basins based on cross plots of Mo and U enrichment factors (e.g., Fig. 6; Algeo and Tribovillard, 2009). U removal from pore water is mediated by Fe- and sulfate-reducing bacteria through reduction of U(VI) to U(IV) and subsequent adsorption or precipitation of uraninite (UO_2) (Klinkhammer and Palmer, 1991; Lovley et al., 1991; Zheng et al., 2002; Liger et al., 2005; Suzuki et al., 2005). As sulfate reduction (and thus Mo removal as thiomolybdate) succeeds Fe reduction during early diagenesis, sedimentary $(Mo/U)_{XS}$ ratios increase with decreasing benthic redox potential (Fig. 6; Algeo and Tribovillard, 2009. Moreover, U has less affinity for adsorption to metal (oxyhydr)oxides compared to Mo (Klinkhammer and Palmer, 1991). Therefore, a high flux of Mn and Fe (oxyhydr)oxides across an oxic-anoxic interface in the water column (i.e., a Mn and Fe shuttle) may lead to a preferential accumulation of Mo relative to U ($(Mo/U)_{XS} > (Mo/U)_{seawater}$) (e.g., Cariaco Basin, Fig. 6; Algeo and Tribovillard, 2009). Finally, in permanently euxinic basins, where intense

scavenging of thiomolybdate and sluggish deep water renewal have led to a preferential depletion of Mo over U in the water column (i.e., $(Mo/U)_{aq} < (Mo/U)_{seawater}$), sediments may be enriched in U relative to Mo ($(Mo/U)_{XS} < (Mo/U)_{seawater}$) (e.g., the Black Sea, Fig. 6; Algeo and Tribovillard, 2009). Consistent with the former two scenarios, pore water and sediment data in the Gotland Deep show an inverse pattern with decreasing $(Mo/U)_{porewater}$ and increasing $(Mo/U)_{XS}$ with increasing water depth (Fig. 7). Moreover, sub-chemocline sediments of the Gotland Deep plot on the trend defined by settings where a Mn and Fe shuttle has been identified (Fig. 6; Algeo and Tribovillard, 2009). This observation suggests that scavenging of Mo by Mn and Fe (oxyhydr)oxides is at least one major vector for Mo delivery to the sediment surface. As noted in Section 5.1, most of the Mn and Fe (oxyhydr)oxides arriving at the seafloor are converted to other authigenic phases during early diagenesis. The result of these phase changes and different reaction pathways during diagenesis means that both the pore fluid and solid phase Mo profiles will likely differ from those of Mn and Fe, particularly below the chemocline.

The three pore water profiles from above the chemocline exhibit Mo removal within the upper few cm, with apparent removal being shallower in the sediment column as the cores progress to greater water depth (Fig. 3). This pattern of removal generally follows that of TH_2S with almost complete Mo depletion in MUC01 (94 m) and MUC11 (111 m) being observed where TH_2S exceeds a few tens of µM (roughly corresponding to a $[H_2S]_{aq}$ of 11 µM). This observation is consistent with the model of Mo scavenging from sulfidic solutions after transformation of MoO_4^{2-} to MoS_4^{2-} (Helz et al., 1996; Erickson and Helz, 2000). In contrast, pore waters of the shallowest core do not reach the $[H_2S]_{aq}$ threshold ($TH_2S \approx 3$ µM at the Mo minimum) and Mo depletion is limited to values of about half the bottom water concentration (Fig. 3). One mechanistic rationale for this observation is that MoO_4^{2-} or intermediate thiomolybdate species dominate in the slightly sulfidic pore water of this core (Helz et al., 1996; Dahl et al., 2010). Oxythiomolybdates are thought to have a smaller affinity for reactive surfaces compared to MoS_4^{2-} (Dahl et al., 2010), which might explain the inefficient Mo removal from pore fluids. In addition, pore waters

of the shallowest core display relatively high dissolved Mn and Fe concentrations and the Mo increase in pore water coincides with a slight increase in dissolved Mn and Fe. Therefore, release of Mo from a Mn- and Fe-rich sediment layer is another possible mechanism limiting Mo depletion in the pore water of this core.

The pore water of cores below the chemocline are the least depleted or even enriched in Mo in certain depth intervals, despite high TH_2S concentrations (Fig. 3) as well as high Mo/Al ratios (Fig. 4). This observation is consistent with an additional source of Mo, possibly associated with Mn and Fe (oxyhydr)oxides. Following prior work (Huckriede and Meischner, 1996; Sternbeck and Sohlenius, 1997; Neumann et al., 1997), we suspect that there is significant Mn as well as some Fe (see section 5.1) supplied to Gotland Deep sediments during oxidation events. Mn- and Fe oxide-rich particles that precipitate at the chemocline of the Gotland Deep are indeed highly enriched in Mo (263 $\mu g\ g^{-1}$; Dellwig et al., 2010) whereas carbonate minerals are generally believed to not incorporate substantial amounts of Mo (<<1 $\mu g\ g^{-1}$; Voegelin et al., 2009). We therefore suspect that the conversion of Mn to rhodochrosite after an inflow event is initially accompanied by the transfer of Mo into solution. Under this scenario, a perhaps significant fraction of the Mo released from Mn (oxyhydr)oxides at the sediment surface is likely to diffuse into the overlying bottom water (see also section 5.4). However, the isolated peaks in dissolved Mo in sub-chemocline cores (Fig. 3) suggest that another fraction of the shuttled Mo is initially buried and some of this Mo is also released into the pore water during early diagenesis. A portion of the Mo released at depth may derive from Fe and Mn (oxyhydr)oxides that have escaped shallow dissolution and transformation to rhodochrosite (Fig. 5), respectively. Moreover, some of the Mo released from Mn (oxyhydr)oxides at the sediment surface might be re-adsorbed by Fe (oxyhydr)oxides (e.g., Scholz et al., 2011; Goldberg et al., 2012) and later released into the pore water upon conversion of Fe (oxyhydr)oxides to Fe sulfides through reaction with H_2S.

We also note that elevated pore water Mo concentrations in sub-chemocline cores coincide with elevated concentrations of dissolved U (Fig. 3). As U delivery with metal (oxyhydr)oxides is thought to be of minor importance (Klinkhammer and Palmer, 1991), additional explanations are necessary to explain their co-variation. Although both U and Mo show a trend towards higher pore water concentrations below the chemocline, the $(Mo/U)_{aq}$ ratio in pore water decreases from the shallower sites into the deep basin (Fig. 7). This observation implies greater mobility of U relative to Mo under the conditions prevailing at the deepest site (MUC05). Such mobility is consistent with prior work showing that in environments with fluctuating redox conditions, authigenic U is highly susceptible to re-mobilization (Zheng et al., 2002; Morford et al., 2009; Scholz et al., 2011) whereas Mo accumulation might be favored by the occasional occurrence of oxidizing conditions (Scholz et al., 2011; Dahl et al., 2013). The latter assumption is grounded on the experimental observation that zero-valent sulfur compounds (chiefly S_8), e.g., forming through incomplete re-oxidation of S(-II) (Rickard and Morse, 2005) at a mobile oxic-anoxic interface, favor the transformation of $Mo(VI)OS_3^{2-}$ to highly particle-reactive Mo(IV)-polysulfide complexes (Vorlicek et al., 2004; Dahl et al., 2013). Preferential delivery of Mo with Mn and Fe (oxyhydr)oxides and preferential remobilization of U are difficult to differentiate as both processes occur during inflow and oxygenation events. Scholz et al. (2011) reported a similar trend of gently increasing Mo and strongly increasing U concentrations in pore water on a sediment core transect across the Peruvian margin. The lowest pore water $(Mo/U)_{aq}$ ratios were observed at the shallowest sites where sediments are most sulfidic but also subject to occasional re-oxidation. Scholz et al. (2011) attributed this observation to enhanced Mo delivery by a Mn and Fe shuttle and preferential remobilization of U during occasional oxic events. A similar mechanism could be anticipated for sub-chemocline sediments of the Gotland Deep.

In general, either organic matter or metal sulfides are considered the final burial phases for Mo in anoxic marine sediments (e.g., Huerta-Diaz and Morse, 1992; Algeo and Lyons, 2006; Helz et al., 2011). The

419 correlation between Mo/Al and Fe/Al or TS is poor (R^2 = 0.001 below the chemocline) suggesting that
420 pyrite or other Fe sulfide minerals are of subordinate importance for Mo burial. In agreement with
421 sediments from many other euxinic basins (Algeo and Lyons, 2006), however, Mo concentrations are
422 well correlated with TOC (MUC04: R^2 = 0.71, n = 15; MUC05: R^2 = 0.83, n = 15). Organic carbon
423 accumulation and preservation is generally more intense under anoxic or euxinic conditions. As a result,
424 TOC concentrations are highest adjacent to the rhodochrosite layers. Much of the Mo bound to organic
425 matter might have been scavenged as thiomolybdate in the water column during euxinic periods (Nägler
426 et al., 2011). However, given the high Mo and H_2S concentrations in the pore water, ongoing
427 sequestration of Mo by organic matter is likely to occur after deposition and during burial. We therefore
428 assume that a significant portion of the Mo delivered by Mn and Fe (oxyhydr)oxides is ultimately buried
429 in association with organic matter.

430 According to the above discussion, the burial flux of Mo is controlled by the following factors: (1) the
431 mass of Mo scavenged by Mn and Fe (oxyhydr)oxides during inflow events; (2) the H_2S concentration in
432 pore water and availability of appropriate organic compounds for the retention of Mo after release from
433 Mn and Fe carrier phases; and (3) the mass of Mo scavenged as thiomolybdate during euxinic periods.
434 The latter two factors have likely become more favorable for Mo accumulation since the late 19th
435 century because of expanding anoxia in the Baltic Deeps (Hille et al., 2006; Zillén et al., 2008; Conley et
436 al., 2009). The progressive shoaling of euxinia over the last century is reflected in the steady increase of
437 Mo/Al and Mo/TOC ratios above 8 cm in the shallower sub-chemocline core (MUC04, 169 m water
438 depth, Fig. 4). The mass of Mo shuttled by Mn and Fe (oxyhydr)oxides should depend on the balance
439 between Mn and Fe accumulation in the deep water during euxinic periods and the frequency of inflow
440 events for re-precipitation and Mo scavenging. In agreement with this hypothesis, Mo/Al and Mo/TOC
441 ratios in the deepest core (MUC05, 223 m) are highest between 12 and 3.5 cm (Fig. 4), i.e., in the depth
442 interval corresponding to the time span between the 1940s to the 1970s. The regular alternation of

stagnation and inflow during this period (Fig. 1D) seems to have been most favorable for Mo accumulation in the deepest part of the Gotland Deep. Decreasing Mo/Al and Mo/TOC ratios above 3.5 cm might reflect the development of more permanent euxinia since the late 1970s. We also note that sediment profiles of U/Al display essentially the same pattern as Mo/Al below the chemocline. As U does not take part in the Mn and Fe shuttle, decreasing solid phase concentrations of U and Mo since the 1970s could also be attributed to a drawdown of these elements in the water column, i.e. the so-called "basin reservoir effect" (Algeo and Lyons, 2006).

5.4. Mechanisms driving the molybdenum inventory of the water column

In 2006, the Gotland Deep water column was depleted in Mo with respect to its conservative distribution ($(Mo)_{conserv}$ - $(Mo)_{aq}$ ≈ 8 nM below ~80 m water depth; Nägler et al., 2011). Assuming that inflow of Mo-replete seawater is the primary source and burial in the sediment the primary sink for Mo, Emerson and Huested (1991) predicted the extent of Mo depletion in the water column of euxinic basins with the following mass balance equation:

$$(\mathrm{Mo})_{\mathrm{SS}} = (\mathrm{Mo})_{\mathrm{conserv}} - \mathrm{F}(\mathrm{Mo})_{\mathrm{XS,burial}} \cdot \frac{\tau_{\mathrm{salinity}}}{z} \quad (3)$$

In this equation $(Mo)_{ss}$ is the Mo concentration at steady state, $(Mo)_{conserv}$ is the conservative Mo concentration normalized to salinity, $F(Mo)_{XS,burial}$ is the Mo burial flux, $\tau_{salinity}$ is the residence time of conservative seawater constituents (equals the mean deep water age) and z is the average thickness of the anoxic water column. The average thickness of the anoxic water column in the Gotland Deep is about 90 m (taking the 150 m isobath as the boundary of the Gotland Deep; Table 3 and Fig. 1B,C). $\tau_{salinity}$ for the Baltic deep water is estimated to be ~20 yr (Reissmann et al., 2009). To account for decreasing sedimentary Mo concentrations with decreasing water depth (Fig. 4), we calculated an area-weighted burial flux that is based on the average MAR below 150 m water depth of Hille et al. (2006) and discrete

Mo concentrations for the seafloor areas between 150 and 200 m and >200 m water depth (Table 3, Fig. 4). Based on these input values we calculate a $(Mo)_{ss}$ of 9.2 nM.

As an alternative to the budgetary approach of Emerson and Huested (1991), a thermodynamic model of Helz et al. (2011) predicts constant deep water Mo concentrations once equilibrium with respect to a nanoparticulate Fe-Mo-S mineral is attained (the proposed stoichiometry equals $Fe_5Mo_3S_{14}$). Prerequisite for the applicability of this model is oversaturation with respect to amorphous Fe monosulfide (Helz et al., 2011). Assuming oversaturation with respect to Fe monosulfide, which is consistent with the environmental state of the Gotland Deep water in 2010 (S = 12.5, pH = 7.3 (Ulfsbo et al., 2011), $(TH_2S)_{aq}$ = 50 µM, $(Fe)_{aq}$ = 1.3 µM (Meyer et al., 2012)), we predict a deep water Mo concentration ($(Mo)_{pred}$) of ~1.5 nM (based on the model of Helz et al., 2011). During the sampling campaign of Nägler et al. (2011), the Gotland Deep was less sulfidic than in 2010, which likely limited oversaturation with respect to Fe monosulfide to water depths below 200 m. The $(Mo)_{aq}$ measured at this depth was 34 nM (Nägler et al., 2011), i.e., the Mo concentrations predicted by the two models are very different and neither equals the observed $(Mo)_{aq}$.

The difference between the observed Mo concentration and the limiting Mo concentration calculated after Helz et al. (2011) may be explained by the short seawater residence time in the Gotland Deep. Relatively fast exchange of the deep water and associated oscillation between oxic and sulfidic conditions may prevent thermodynamic equilibrium with respect to nanoparticulate Fe-Mo-S. Consistent with this rationale, a similarly large offset between $(Mo)_{pred}$ and $(Mo)_{aq}$ has been reported for other weakly restricted euxinic systems, e.g. in the Cariaco Basin and Saanich Inlet (Helz et al., 2011). Similarly, some of the offset between the observed Mo concentration and the steady state Mo concentration (Eq. (3)) could be related to the relatively recent inflow event of 2003 (Fig. 1D). The majority of deep water renewal in the Gotland Deep takes place during inflow events rather than through continuous vertical exchange (without inflow events $\tau_{salinity}$ would be on the order of 100 yr;

Feistel et al., 2006). As a result, most seawater constituents whose concentrations decrease during stagnant periods because of microbial metabolism or other biogeochemical processes experience a linear drawdown between inflow events (Matthäus et al., 2008). In the case of Mo, the mean slope or velocity of this drawdown is given by $((Mo)_{SS}-(Mo)_{conserv})/\tau_{salinity}$ (in nmol yr^{-1}). According to this equation, a linear drop in the deep water Mo concentration by 8 nM (Nägler et al., 2011) requires a stagnant period of ~4.7 yr. This result would imply that the isolated inflow event of 2003 was accompanied by an almost complete exchange of the Gotland Deep water, which appears to be unlikely. Instead we propose that the Mo inventory of the deep water is buffered by two additional recharge mechanisms that are not considered in Eq. (3). As pointed out by Dellwig et al. (2010), the continuous cycle of Mn (oxyhydr)oxide precipitation at the chemocline and reductive dissolution in the euxinic water mass is likely to maintain a constant Mo flux into the deep water. Furthermore, our pore water and sediment results suggest that Mo removal and burial does not only take place during euxinic periods but also during inflow events. As mentioned earlier, much of the Mo scavenged during inflow events is likely to become recycled into the bottom water thus buffering its Mo inventory. Further evidence for Mo recycling in the aftermath of an inflow event is provided by water column Mo data from Prange and Kremling (1986). These data were obtained in 1979, i.e. shortly after the extended period of inflows from 1968 to 1978 (Fig. 1D). At this time, the Mo concentration in the Gotland Deep water was conservative (41.6 nM) up to 200 m water depth but as high as 46 nM below (Prange and Kremling, 1986). Using a modified version of Eq. (3), we can estimate the backflux of Mo that is required to achieve this concentration within the time elapsed since the last inflow event:

$$F(Mo)_{back} = \left((Mo)_{conserv} - (Mo)_{aq,1979}\right) \cdot \frac{z}{\tau_{1979\text{-}1978}} \quad (4)$$

In this equation, z is the average thickness of the water column below 200 m water depth (~18 m; Table 3) and $\tau_{1979\text{-}1978}$ is the time span between the last inflow event in 1978 and the sampling campaign in

512 1979 (~1.5 yr). The resulting $F(Mo)_{back}$ of $-0.53 \cdot 10^5$ nmol m^{-2} yr^{-1} (the negative sign indicates an upward
513 flux) is in good agreement with published benthic Mo fluxes from manganous or ferruginous sediments
514 that were calculated based on pore water concentration gradients (e.g., $\geq -2.5 \cdot 10^5$ nmol m^{-2} yr^{-1} in the
515 Santa Barbara Basin; Zheng et al., 2000; $\geq -2.0 \cdot 10^5$ nmol m^{-2} yr^{-1} on the Peruvian shelf; Scholz et al,
516 2011). Recycling of shuttled Mo after inflow events could be particularly important for buffering the Mo
517 inventory of the deepest water layer where Mo scavenging during euxinic periods is likely to be most
518 intense.

519 **5.5. Further implications for the use of molybdenum as an ocean redox proxy**

520 Published δ^{98}Mo data for sediments in the Gotland Deep range between +0.4 and +0.6 ‰ (Neubert et
521 al., 2008). These isotope values differ from the modern seawater isotope composition (δ^{98}Mo = 2.3 ‰),
522 which is consistent with the idea that there is incomplete removal of a fractionated Mo pool from the
523 water column. One likely mechanism contributing to the isotopic offset between sediment and seawater
524 ($\Delta^{98}Mo_{seawater\text{-}sediment} \approx +1.8$ ‰) is the scavenging of intermediate thiomolybdate species during euxinic
525 periods (e.g., Nägler et al., 2011). Nägler et al. (2011) hypothesized that occasional inflow of oxic
526 seawater perturbs the transformation of $MoOS_3^{2-}$ to MoS_4^{2-}. As the progressive transformation of MoO_4^{2-}
527 to MoS_4^{2-} is accompanied by isotope fractionation (Tossel, 2005), scavenging of intermediate
528 thiomolybdate species should result in a greater isotopic offset between seawater and sediment than
529 scavenging of MoS_4^{2-} alone (Nägler et al., 2011). Both previous (Dellwig et al., 2010) and our new
530 findings on Mo cycling in the Gotland Deep suggest that a portion of the sedimentary Mo is shuttled by
531 Mn and Fe (oxyhydr)oxides. The isotopically light Mo pool resulting from this transport mechanism is
532 likely to contribute to the Mo isotopic offset between sediments and seawater (see also Nägler et al.,
533 2011).

As observed in the Gotland Deep (Nägler et al., 2011), sediments of weakly restricted or intermittently euxinic basins often display an isotopic offset with respect to the Mo isotope composition of seawater (e.g., Cariaco Basin; Arnold et al., 2004). A common explanation for this offset is lower H_2S concentrations and thus less efficient conversion of MoO_4^{2-} to MoS_4^{2-} compared to the strongly and permanently sulfidic Black Sea (Neubert et al., 2008; Dahl et al., 2010). In addition, Dahl et al. (2010) pointed out that a short seawater residence time limits the progress of the MoO_4^{2-} to MoS_4^{2-} conversion and thus increases the isotopic offset between scavenged and dissolved Mo. Our work further emphasizes the role of Mn and Fe (oxyhydr)oxides in generating a light Mo isotope signature in euxinic systems with a short seawater residence time. Repeated inflow of oxic water or continuous mixing of oxic and anoxic water increases the frequency of Mn and Fe precipitation and re-dissolution (see sketch in Fig. 8A). The high Mo burial rates that are typically observed in weakly restricted euxinic basins with a short seawater residence time (i.e., Saanich Inlet, Cariaco Basin) have been assigned to this shuttle mechanism (Algeo and Lyons, 2006).

We further suggest that accelerated Mo burial in association with a Mn and Fe shuttle is not necessarily restricted to isolated basins, but may operate on open-marine continental margins as well, provided that an oxic-anoxic interface for Mn and Fe redox cycling is available. For instance, intense Mo burial and $(Mo/U)_{XS} > (Mo/U)_{seawater}$ (Fig. 6) in shelf sediments underlying the Peruvian oxygen minimum zone have been attributed to such a mechanism (Scholz et al., 2011). Furthermore, it is possible that such a shuttle operated at euxinic ocean margins in early Earth history. By analogy to the oxygen minimum zones of coastal upwelling areas in the modern ocean, a number of recent studies inferred localized euxinia underneath oxic surface waters for ocean margins in the late Archean (Reinhard et al, 2009; Kendall et al., 2010) and the Proterozoic (Poulton et al., 2010; Li et al., 2010; Poulton and Canfield, 2011). Euxinic water masses are generally enriched in Mn and Fe compared to oxic water masses (Saito et al, 2003) and it has been suggested that redox boundaries in the Proterozoic were subject to

558 considerable fluctuation (Johnston et al., 2010; Poulton et al., 2010). These factors, along with the short
559 seawater residence time at open-marine margins, likely favored the rapid redox cycling of Mn and Fe.
560 Euxinic conditions in the water column overlying the continental shelf (Poulton et al., 2010; Li et al.,
561 2010) should thus have promoted a Mn and Fe shuttle that efficiently transported Mo from the
562 chemocline to the sediment (see sketch in Fig. 8B). By analogy to modern weakly restricted basins or
563 continental margin environments (Siebert et al., 2006; Poulson Brucker et al., 2009), the Proterozoic Mn
564 and Fe shuttle would have likely generated an offset in δ^{98}Mo between the sediment and contemporary
565 seawater.

566 At the same time, the short seawater residence time likely limited the potential for Mo depletion within
567 the local water column; for example, typical wind-driven upwelling rates on continental shelves are on
568 the order of meters per day corresponding to seawater residence times ($\tau_{salinity}$) of tens of days (Bowden,
569 1977). Applying a $\tau_{salinity}$ of 50 days and an average OMZ thickness of 150 m (e.g., Keeling et al., 2011) to
570 Eq. (3) yields a $(Mo)_{SS}$ of 41.5 nM, which is analytically indistinguishable from $(Mo)_{conserv}$. Importantly, the
571 relative extent of Mo depletion at steady state is largely independent of $(Mo)_{conserv}$ and, within the limits
572 defined by modern euxinic environments (Algeo and Lyons, 2006), of $F(Mo)_{XS,burial}$. This result implies
573 that localized euxinic water bodies at ocean margins were unlikely depleted in Mo with respect to
574 contemporary seawater or that in contrast to the deep Black Sea, residual Mo in the water column could
575 likely escape precipitation along open-marine euxinic systems. Moreover, the short seawater residence
576 time likely prevented the complete conversion of MoO_4^{2-} to MoS_4^{2-} (Dahl et al., 2010). The ultimate
577 prerequisite for open-marine euxinic sediments to record the δ^{98}Mo of seawater thus seems to be
578 widespread euxinia in the deep-ocean, which results in complete sulfidation of molybdate prior to
579 upwelling on the continental shelf. However, the concept of persistent deep-ocean euxinia in the
580 Proterozoic is increasingly superseded by the notion of euxinic intermediate waters sandwiched
581 between ferruginous deep water and oxic surface water (Li et al., 2010; Poulton et al, 2010; Dahl et al.,

582 2011; Poulton and Canfield, 2011). We suggest that this "oxygen minimum zone-type" redox-structure
583 may not allow for a $\Delta^{98}Mo_{seawater\text{-}sediment}$ of zero. By contrast, the occurrence and intensity of the Mn and
584 Fe shuttle at euxinic continental margins is independent of the redox state of the deep-ocean.
585 Accordingly, continental margin sediment facies with a light Mo isotope signature ($\delta^{98}Mo < 2.3$ ‰) and
586 independent evidence for euxinia (e.g., from Fe proxies) does not necessarily reflect Mo depletion on a
587 global scale, but could instead result from Mo transport via a Mn and Fe shuttle.

588 **6. Conclusions**

589 Euxinic sediments of the Gotland Deep in the Baltic Sea were investigated with the aim of characterizing
590 geochemical processes that lead to Mo accumulation. Our data reveal that multiple mechanisms are
591 likely contributing to Mo burial, including scavenging of thiomolybdate (or other Mo-sulfide-complexes)
592 or Fe-Mo-S nanoparticles by organic matter during euxinic periods and adsorption of molybdate by Mn
593 and Fe (oxyhydr)oxides during more oxic periods. The latter mechanism is primarily driven by inflow and
594 oxygenation events during which dissolved Mn and Fe that has accumulated within the euxinic deep
595 water is oxidized and deposited at the basin floor. This Mn and Fe shuttle is a common feature in weakly
596 restricted basins. We suggest that Mo isotope fractionation associated with adsorption of Mo onto Mn
597 and Fe (oxyhydr)oxides contributes to the Mo isotopic offset from seawater that is commonly observed
598 in the sediments of these systems

599 The occurrence of a Mn and Fe shuttle requires a water column redox boundary separating water
600 masses with differing solubility of Mn and Fe as well as rapid turnover of water (corresponding to a
601 short seawater residence time) to maintain intense redox cycling of Mn and Fe. These requirements are
602 not only met in weakly restricted basins but also at the oxygen minimum zones of modern continental
603 margins and, possibly, at sulfidic ocean margins during Earth history. A Mn and Fe shuttle, along with

604 Mo isotope fractionation during adsorption, could thus contribute to the light Mo isotope composition
605 recorded in Proterozoic black shales.

606 **Acknowledgments**

607 Thanks are due to the officers and crew of RV Alkor, the chief scientist Olaf Pfannkuche and the
608 shipboard scientific party for their support during ALK355. We also thank our colleagues Anke Bleyer,
609 Maike Dibbern, Bettina Domeyer, Jesse Muratli, Regina Surberg and Andy Ungerer for manifold help in
610 the labs at Kiel and Corvallis. Anna Noffke is acknowledged for providing salinity, oxygen and H_2S data
611 for the water column. We greatly appreciate thoughtful comments by Tom Jilbert and one anonymous
612 reviewer. Funding was provided by the 7th Framework Program of the European Union (HYPOX project,
613 Grant Agreement No. 226213; Marie Curie IOF to FS, BICYCLE, Grant Agreement No. 300648). US
614 National Science Foundation Grant No. 1029889 supported the participation of JM.

615 **References**

616 Algeo, T.J., Lyons, T.W., 2006. Mo-total organic carbon covariation in modern anoxic marine
617 environments: Implications for analysis of paleoredox and paleohydrographic conditions.
618 Paleoceanography, 21, PA1016, doi:10.1029/2004PA001112.

619 Algeo, T.J., Tribovillard, N., 2009. Environmental analysis of paleoceanographic systems based on
620 molybdenum-uranium covariation. Chem. Geol., 268, 211-225.

621 Archer, C, Vance, D., 2008. The isotopic signature of the global riverine molybdenum flux and anoxia in
622 the ancient oceans. Nature Geosci., 1, 597-600.

623 Arnold, G.L., Anbar, A.D., Barling, J., Lyons, T.W., 2004. Molybdenum isotope evidence for widespread
624 anoxia in mid-proterozoic oceans. Science, 304, 87-90.

625 Barling, J., Arnold, G.L., Anbar, A.D., 2001. Natural mass-dependent variations in the isotopic
626 composition of molybdenum. Earth Planet. Sci. Lett., 193, 447-457.

627 Barling, J., Anbar, A.D., 2004. Molybdenum isotope fractionation during adsorption by manganese
628 oxides. Earth Planet. Sci. Lett., 217, 315-329.

629 Berrang, P.G., Grill, E.V., 1974. The effect of manganese oxide scavenging on molybdenum in saanich
630 inlet, British Columbia. Mar. Chem., 2, 125-148.

631 Boesen, C., Postma, D., 1988. Pyrite formation in anoxic environments of the Baltic. Am. J. Sci., 288, 575-
632 603.

633 Bostick, B.C., Fendorf, S., Helz, G.R., 2003. Differential adsorption of molybdate and tetrathiomolybdate
634 on pyrite (FeS_2). Environ. Sci. Technol., 37, 285-291.

635 Bowden, K.F., 1977. Heat budget considerations in the study of upwelling, in: Angel, M. (Ed.), A voyage
636 of discovery. Pergamon Press, Oxford, 277-290.

637 Bruland, K.W., 1983. Trace elements in sea-water, in: eds. Riley, J. P., Chester, R. (Eds.), Chemical
638 oceanography. Academic Press, London, 157-220.

639 Burdige, D.J., 1993. The biogeochemistry of manganese and iron reduction in marine sediments. Earth-
640 Sci. Rev., 35, 249-284.

641 Canfield, D.E., Thamdrup, B., Hansen, J.W., 1993. The anaerobic degradation of organic matter in Danish
642 coastal sediments: Iron reduction, manganese reduction, and sulfate reduction. Geochim.
643 Cosmochim. Acta, 57, 3867-3883.

644 Cartapanis, O., Tachikawa, K., Bard, E., 2011. Northeastern Pacific oxygen minimum zone variability over
645 the past 70 kyr: Impact of biological production and oceanic ventilation. Paleoceanography, 26,
646 PA4208, doi: 10.1029/2011PA002126.

647 Chan, K.M., Riley, J.P., 1966. The determination of molybdenum in natural waters, silicates and
648 biological materials. Anal. Chim. Acta, 36, 220-229.

649 Conley, D.J., Björck, S., Bonsdorff, E., Carstensen, J., Destouni, G., Gustafsson, B.G., Hietanen, S.,
650 Kortekaas, M., Kuosa, H., Meier, H. E.M., Müller-Karulis, B., Nordberg, K., Norkko, A., Nürnberg, G.,
651 Pitkänen, H., Rabalais, N.N., Rosenberg, R., Savchuk, O.P., Slomp, C.P., Voss, M., Wulff, F., Zillén, L.,
652 2009. Hypoxia-related processes in the Baltic Sea. Environ. Sci. Technol., 43, 3412-3420.

653 Dahl, T.W., Anbar, A.D., Gordon, G.W., Rosing, M.T., Frei, R., Canfield, D.E., 2010. The behavior of
654 molybdenum and its isotopes across the chemocline and in the sediments of sulfidic Lake Cadagno,
655 Switzerland. Geochim. Cosmochim. Acta, 74, 144-163.

656 Dahl, T.W., Canfield, D.E., Rosing, M.T., Frei, R.E., Gordon, G., Knoll, A., Anbar, A.D., 2011. Molybdenum
657 evidence for expansive sulfidic water masses in ~750 Ma oceans. Earth Planet. Sci. Lett., 311, 264-
658 274.

659 Dahl, T.W., Chappaz, A., Fitts, J.P., Lyons, T.W., 2013. Molybdenum reduction in a sulfidic lake: Evidence
660 from X-ray absorption fine-structure spectroscopy and implications for the Mo paleoproxy.
661 Geochim. Cosmochim. Acta, 103, 213-231.

662 Dellwig, O., Leipe, T., März, C., Glockzin, M., Pollehne, F., Schnetger, B., Yakushev, E.V., Böttcher, M.E.,
663 Brumsack, H.J., 2010. A new particulate Mn-Fe-P-shuttle at the redoxcline of anoxic basins.
664 Geochim. Cosmochim. Acta, 74, 7100-7115.

665 Emerson, S.R., Huested, S.S., 1991. Ocean anoxia and the concentrations of molybdenum and vanadium
666 in seawater. Mar. Chem., 34, 177-196.

667 Erickson, B.E., Helz, G.R., 2000. Molybdenum(VI) speciation in sulfidic waters: Stability and lability of
668 thiomolybdates. Geochim. Cosmochim. Acta, 64, 1149-1158.

669 Feistel, R., Nausch, G. and Hagen, E., 2006. Unusual Baltic inflow activity in 2002-2003 and varying deep-
670 water properties. Oceanologia, 48, 21-35.

671 Fehr, M.A., Andersson, P.S., Halenius, U., Mörth, C.M., 2008. Iron isotope variations in Holocene
672 sediments of the Gotland Deep, Baltic Sea. Geochim. Cosmochim. Acta, 72, 807-826.

673 Froelich, P.N., Klinkhammer, G.P., Bender, M.L., Luedtke, N.A., Heath, G.R., Cullen, D., Dauphin, P.,
674 Hammond, D., Hartmann, B., Maynard, V., 1979. Early oxidation of organic matter in pelagic
675 sediments of the eastern equatorial Atlantic: suboxic diagenesis. Geochim. Cosmochim. Acta, 43,
676 1075-1090.

677 Goldberg, T., Archer, C., Vance, D., Poulton, S.W., 2009. Mo isotope fractionation during adsorption to
678 Fe (oxyhydr)oxides. Geochim. Cosmochim. Acta, 73, 6502-6516.

679 Goldberg, T., Archer, C., Vance, D., Thamdrup, B., McAnena, A., Poulton, S.W., 2012. Controls on Mo
680 isotope fractionations in a Mn-rich anoxic marine sediment, Gullmar Fjord, Sweden. Chem. Geol.,
681 296-297, 73-82.

682 Govindaraju, K., 1994. Compilation of working values and sample description of for 383 geostandards.
683 Geostandard Newslett. 18, 1-158.

684 Grasshoff K., Erhardt, M., Kremling, K., 2002. Methods of seawater analysis. Wiley VCH, Weinheim.

685 Hanninen, J., Vuorinen, I., Hjelt, P., 2000. Climatic Factors in the Atlantic Control the Oceanographic and
686 Ecological Changes in the Baltic Sea. Limnol. Oceanogr., 45, 703-710.

687 Heiser, U., Neumann, T., Scholten, J., Stüben, D., 2001. Recycling of manganese from anoxic sediments
688 in stagnant basins by seawater inflow: a study of surface sediments from the Gotland Basin, Baltic
689 Sea. Mar. Geol., 177, 151-166.

690 Helz, G.R., Miller, C.V., Charnoch, J.M., Mosselmans, J.F.W., Pattrick, R.A.D., Garner, C.D., Vaughan, D.J.,
691 1996. Mechanism of molybdenum removal from the sea and its concentration in black shales:
692 EXAFS evidence. Geochim. Cosmochim. Acta, 60, 3631-3642.

693 Helz, G.R., Bura-Nakić, E., Mikac, N., Ciglenečki, I., 2011. New model for molybdenum behavior in euxinic
694 waters. Chem. Geol., 284, 323-332.

695 Hille, S., Leipe, T., Seifert, T., 2006. Spatial variability of recent sedimentation rates in the Eastern
696 Gotland Basin (Baltic Sea). Oceanologia, 48, 297-317.

697 Huckriede, H., Meischner, D., 1996. Origin and environment of manganese-rich sediments within black-
698 shale basins. Geochim. Cosmochim. Acta, 60, 1399-1413.

699 Huerta-Diaz, M.A., Morse, J.W., 1992. Pyritization of trace metals in anoxic marine sediments. Geochim.
700 Cosmochim. Acta, 56, 2681-2702.

701 Hurrell, J.W., 1995. Decadal Trends in the North Atlantic Oscillation: Regional Temperatures and
702 Precipitation. Science, 269, 676-679.

703 Hurrell, J., Van Loon, H., 1997. Decadal variations in climate associated with the North Atlantic
704 Oscillation. Climatic Change, 36, 301-326.

705 Jakobsen, R., Postma, D., 1989. Formation and solid solution behavior of Ca-rhodochrosites in marine
706 muds of the Baltic deeps. Geochim. .Cosmochim. Acta, 53, 2639-2648.

707 Jilbert, T., Slomp, C.P., 2013. Iron and manganese shuttles control the formation of authigenic
708 phosphorus minerals in the euxinic basins of the Baltic Sea. Geochim. Cosmochim. Acta, 107, 155-
709 169.

710 Johnston, D.T., Poulton, S.W., Dehler, C., Porter, S., Husson, J., Canfield, D.E., Knoll, A.H., 2010. An
711 emerging picture of Neoproterozoic ocean chemistry: Insights from the Chuar Group, Grand
712 Canyon, USA. Earth Planet. Sci. Lett., 290, 64-73.

713 Keeling, R.F., Körtzinger, A., Gruber, N., 2011. Ocean deoxygenation in a warming world. Ann. Rev. Mar.
714 Sci., 2, 199-229.

715 Kendall, B., Creaser, R.A., Gordon, G.W., Anbar, A.D., 2009. Re-Os and Mo isotope systematics of black
716 shales from the Middle Proterozoic Velkerri and Wollogorang Formations, McArthur Basin,
717 northern Australia. Geochim. Cosmochim. Acta, 73, 2534-2558.

718 Kendall, B., Reinhard, C.T., Lyons, T.W., Kaufmann, A.J., Poulton, S.W., Anbar, A.D., 2010. Pervasive
719 oxygenation along late Archaean ocean margins. Nature Geosci., 3, 647-652.

720 Klinkhammer, G.P., Palmer, M.R., 1991. Uranium in the oceans - where it goes and why. Geochim.
721 Cosmochim. Acta, 55, 1799-1806.

722 Leipe, T., Tauber, F., Vallius, H., Virtasalo, J., Uscinowicz, S., Kowalski, N., Hille, S., Lindgren, S.,
723 Myllyvirta., 2011. Particulate organic carbon (POC) in surface sediments of the Baltic Sea. Geo-Mar.
724 Lett., 31, 175-188.

725 Li, C. Love, G.D., Lyons, T.W., Fike, D., Sessions, A.L., Chu, X., 2010. A stratified redox model for the
726 Ediacaran Ocean. Science, 328, 80-83.

727 Liger, E., Charlet, L., Van Cappellen, P., 1999. Surface catalysis of uranium(VI) reduction by iron(II).
728 Geochim. Cosmochim. Acta, 63, 2939-2955.

729 Lovley, D.R., Phillips, E.J.P., Gorby, Y.A., Landa, E.R., 1991. Microbial reduction of uranium. Nature, 350,
730 413-416.

731 Lyons, T.W., Severmann, S., 2006. A critical look at iron paleoredox proxies: New insights from modern
732 euxinic marine basins. Geochim. Cosmochim. Acta, 70, 5698-5722.

733 Matthäus, W., Franck, H., 1992. Characteristics of major Baltic inflows - a statistical analysis. Cont. Shelf
734 Res., 12, 1375-1400.

735 Matthäus, W., Nehring, D., Feistel, R., Nausch, G., Mohrholz, V., Lass, H.U., 2008. The inflow of highly
736 saline water into the Baltic Sea, in: Feistel, R., Nausch, G., Wasmund, N. (Eds.), State and Evolution
737 of the Baltic Sea, 1952 – 2005. A detailed 50-year survey of meteorology and climate, physics,
738 chemistry, biology, and marine environment. John Wiley & Sons, Hoboken, 265-309.

739 McLennan, S.M., 2001. Relationships between the trace element composition of sedimentary rocks and
740 upper continental crust. Geochem. Geophys. Geosyst., 2, Paper number 2000GC000109.

741 McManus, J., Berelson, W.M., Severmann, S., Poulson, R.L., Hammond, D.E., Klinkhammer, G.P., Holm,
742 C., 2006. Molybdenum and uranium geochemistry in continental margin sediments: Paleoproxy
743 potential. Geochim. Cosmochim. Acta, 70, 4643-4662.

744 Meyer, D., Prien, R.D., Dellwig, O., Connelly, D.P., Schulz-Bull, D.E., 2012. In situ determination of iron(II)
745 in the anoxic zone of the central Baltic Sea using ferene as spectrophotometric reagent. Mar.
746 Chem., 130-131, 21-27.

747 Morford, J.L., Emerson, S.R., Breckel, E.J., Kim, S.H., 2005. Diagenesis of oxyanions (V, U, Re, and Mo) in
748 pore waters and sediments from a continental margin. Geochim. Cosmochim. Acta, 69, 5021-5032.

749 Morford, J.L., Martin, W.R., Carney, C.M., 2009. Uranium diagenesis in sediments underlying bottom
750 waters with high oxygen content. Geochim. Cosmochim. Acta, 73, 2920-2937.

751 Muratli, J.M., McManus, J., Mix, A., Chase, Z., 2012. Dissolution of fluoride complexes following
752 microwave-assisted hydrofluoric acid digestion of marine sediments. Talanta, 89, 195-200.

753 Nägler, T.F., Neubert, N., Böttcher, M.E., Dellwig, O., Schnetger, B., 2011. Molybdenum isotope
754 fractionation in pelagic euxinia: Evidence from the modern Black and Baltic Seas. Chem. Geol., 289,
755 1-11.

756 Neretin, L.N., Pohl, C., Jost, G., Leipe, T., Pollehne, F., 2003. Manganese cycling in the Gotland Deep,
757 Baltic Sea. Mar. Chem., 82, 125-143.

758 Neubert, N., Nägler, T.F., Böttcher, M.E., 2008. Sulfidity controls molybdenum isotope fractionation into
759 euxinic sediments: Evidence from the modern Black Sea. Geology, 36, 775-778.

760 Neumann, T., Christiansen, C., Clasen, S., Emeis, K.C., Kunzendorf, H., 1997. Geochemical records of salt-
761 water inflows into the deep basins of the Baltic Sea. Cont. Shelf Res., 17, 95-115.

762 Neumann, T., Heiser, U., Leosson, M.A., Kersten, M., 2002. Early diagenetic processes during Mn-
763 carbonate formation: evidence from the isotopic composition of authigenic Ca-rhodochrosites of
764 the Baltic Sea. Geochim. Cosmochim. Acta, 66, 867-879.

765 Parkhurst, D.L., Appelo, C.A.J., 1999. User's guide to PHREEQC (version 2) - A computer program for
766 speciation, batch-reaction, one-dimensional transport, and inverse geochemical calculations. U.S.
767 Geological Survey Water-Resources Investigations Report 99-4259.

768 Pohl, C. and Fernández-Otero, E., 2012. Iron distribution and speciation in oxic and anoxic waters of the
769 Baltic Sea. Mar. Chem., 145-147, 1-15.

770 Poulson Brucker, R.L., McManus, J., Severmann, S., Berelson, W.M., 2009. Molybdenum behavior during
771 early diagenesis: insights from Mo isotopes. Geochem. Geophys. Geosyst., 10, Q06010,
772 doi:10.1029/2008GC002180.

773 Poulson Brucker, R.L., McManus, J., Poulton, S.W., 2012. Molybdenum isotope fractionations observed
774 under anoxic experimental conditions. Geochem. J., 46, 201-209.

775 Poulton, S.W., Fralick, P.W., Canfield, D.E., 2010. Spatial variability in oceanic redox structure 1.8 billion
776 years ago. Nature Geosci., 3, 486-490.

777 Poulton, S.W., Canfield, D.E., 2011. Ferruginous conditions: a dominant feature of the ocean through
778 Earth's history. ELEMENTS, 7, 107-112.

779 Prange, A. and Kremling, K., 1985. Distribution of dissolved molybdenum, uranium and vanadium in
780 Baltic Sea waters. Mar. Chem., 16, 259-274.

781 Raiswell, R., Anderson, T.F., 2005. Reactive iron enrichment in sediments deposited beneath euxinic
782 bottom waters: constraints on supply by shelf recycling. Geol. Soc. Spec. Publ., 248, 179-194.

783 Reinhard, C.T., Raiswell, R., Scott, C., Anbar, A.D., Lyons, T.W., 2009. A Late Archean sulfidic sea
784 stimulated by early oxidative weathering of the continents. Science, 326, 713-716.

785 Reissmann, J.H., Burchard, H., Feistel, R., Hagen, E., Lass, H.U., Mohrholz, V., Nausch, G., Umlauf, L.,
786 Wieczorek, G., 2009. Vertical mixing in the Baltic Sea and consequences for eutrophication - a
787 review. Prog. Oceanogr., 82, 47-80.

788 Rickard, D., Morse, J.W., 2005. Acid volatile sulfide (AVS). Mar. Chem., 97, 141-197.

789 Saito, M.A., Sigman, D.M., Morel, F.o.M.M., 2003. The bioinorganic chemistry of the ancient ocean: the
790 co-evolution of cyanobacterial metal requirements and biogeochemical cycles at the Archean-
791 Proterozoic boundary? Inorg. Chim. Acta, 356, 308-318.

792 Schinke, H., Matthäus, W., 1998. On the causes of major Baltic inflows - an analysis of long time series.
793 Cont. Shelf Res., 18, 67-97.

794 Scholz, F., Neumann, T., 2007. Trace element diagenesis in pyrite-rich sediments of the Achterwasser
795 lagoon, SW Baltic Sea. Mar. Chem., 107, 516-532.

796 Scholz, F., Hensen, C., Noffke, A., Rohde, A., Liebetrau, V., Wallmann, K., 2011. Early diagenesis of redox-
797 sensitive trace metals in the Peru upwelling area: response to ENSO-related oxygen fluctuations in
798 the water column. Geochim. Cosmochim. Acta, 75, 7257-7276.

799 Scott, C., Lyons, C., Bekker, A., Shen, Y., Poulton, S.W., Chu, X., Anbar, A.D., 2008. Tracing the stepwise
800 oxygenation of the Proterozoic ocean. Nature, 452, 456-459.

801 Shaw, T.J., Gieskes, J.M., Jahnke, R.A., 1990. Early diagenesis in differing depositional environments: The
802 response of transition metals in pore water. Geochim. Cosmochim. Acta, 54, 1233-1246.

803 Seifert, T., Tauber, F., Kayser, B, 2001. A high resolution spherical grid topography of the Baltic Sea – 2nd
804 edition. Baltic Sea Science Congress, Stockholm 25-29. November 2001, Poster #147.

805 Shimmield, G.B., Price, N.B., 1986. The behaviour of molybdenum and manganese during early sediment
806 diagenesis - offshore Baja California, Mexico. Mar. Chem., 19, 261-280.

807 Siebert, C., Nägler, T.F., von Blanckenburg, F., Kramers, J.D., 2003. Molybdenum isotope records as a
808 potential new proxy for paleoceanography. Earth Planet. Sci. Lett., 211, 159-171.

809 Siebert, C., McManus, J., Bice, A., Poulson, R., Berelson, W.M., 2006. Molybdenum isotope signatures in
810 continental margin marine sediments. Earth Planet. Sci. Lett., 241, 723-733.

811 Sternbeck, J., Sohlenius, G., 1997. Authigenic sulfide and carbonate mineral formation in Holocene
812 sediments of the Baltic Sea. Chem. Geol., 135, 55-73.

813 Suess, E., 1979. Mineral phases formed in anoxic sediments by microbial decomposition of organic
814 matter. Geochim. Cosmochim. Acta, 43, 339-352.

815 Suzuki, Y., Kelly, S.D., Kemner, K.M., Banfield, J.F., 2005. Direct microbial reduction and subsequent
816 preservation of uranium in natural near-surface sediment. Appl. Environ. Microbiol., 71, 1790-
817 1797.

818 Tossell, J.A., 2005. Calculating the partitioning of the isotopes of Mo between oxidic and sulfidic species
819 in aqueous solution. Geochim. Cosmochim. Acta, 69, 2981-2993.

820 Tribovillard, N., Riboulleau, A., Lyons, T.W., Baudin, F., 2004. Enhanced trapping of molybdenum by
821 sulfurized marine organic matter of marine origin in Mesozoic limestones and shales. Chem. Geol.,
822 213, 385-401.

823 Ulfsbo, A., Hulth, S., Anderson, L.G., 2011. pH and biogeochemical processes in the Gotland Basin of the
824 Baltic Sea. Mar. Chem., 127, 20-30.

825 Visbeck, M.H., Hurrell, J.W., Polvani, L., Cullen, H.M., 2001. The North Atlantic Oscillation: Past, present,
826 and future. P. Natl. Acad. Sci. USA, 98, 12876-12877.

827 Voegelin, A.R., Nägler, T.F., Samankassou, E., Villa, I.M., 2009. Molybdenum isotopic composition of
828 modern and Carboniferous carbonates. Chem. Geol., 265, 488-498.

829 Vorlicek, T.P., Helz, G.R., 2002. Catalysis by mineral surfaces: Implications for Mo geochemistry in anoxic
830 environments. Geochim. Cosmochim. Acta, 66, 3679-3692.

831 Vorlicek, T.P., Kahn, M.D., Kasuya, Y., Helz, G.R., 2004. Capture of molybdenum in pyrite-forming
832 sediments: Role of ligand-induced reduction by polysulfides. Geochim. Cosmochim. Acta, 68, 547-
833 556.

834 Wasylenki, L.E., Rolfe, B.A., Weeks, C.L., Spiro, T.G., Anbar, A.D., 2008. Experimental investigation of the
835 effects of temperature and ionic strength on Mo isotope fractionation during adsorption to
836 manganese oxides. Geochim. Cosmochim. Acta, 72, 5997-6005.

837 Zheng, Y., Anderson, R.F., van Geen, A. and Kuwabara, J., 2000. Authigenic molybdenum formation in
838 marine sediments: A link to pore water sulfide in the Santa Barbara Basin. Geochim. Cosmochim.
839 Acta, 64, 4165-4178.

840 Zheng, Y., Anderson, R.F., Van Geen, A., Fleisher, M.Q., 2002. Remobilization of authigenic uranium in
841 marine sediments by bioturbation. Geochim. Cosmochim. Acta, 66, 1759-1772.

842 Zillén, L., Conley, D.J., Andrén, T., Andrén, E., Björck, S., 2008. Past occurrences of hypoxia in the Baltic
843 Sea and the role of climate variability, environmental change and human impact. Earth-Sci. Rev.,
844 91, 77-92.

845 **Figure captions**

846 Figure 1. (A) Bathymetric map of the Baltic Sea (bathymetric data from Seifert et al., 2001). (B) Close-up
847 showing the Gotland Deep and the location of coring sites (red stars). (C) Bathymetric cross section
848 through the Baltic Sea from the Danish Straits to the Gotland Deep (see solid line in (A)). (D) Record of
849 Major Baltic Inflows (MBI) from 1930 till present. Groups of events are depicted by gray areas and single
850 events are depicted by gray lines. Red stars in (D) represent the time of sampling campaigns in the
851 Gotland Deep that are relevant to this study.

852 Figure 2. Profiles of salinity, oxygen and TH_2S in the water column of the Gotland Deep during May and
853 June 2010 (A. Noffke, unpublished data). The location of the chemocline and coring sites are depicted on
854 the right-hand side.

855 Figure 3. Pore water profiles of salinity (calculated from Cl^-), SO_4^{2-} (black circles), TH_2S (open circles), Mn
856 (black circles), Fe (open circles), Mo and U. The uppermost value of each profile (depth = 0 cm) indicates
857 bottom water concentrations. Vertical dashed lines represent conservative SO_4^{2-}, Mo and U
858 concentrations as calculated from Cl^-. The horizontal arrow between MUC11 and MUC04 indicates the
859 location of the chemocline. The very high Mo and U concentration in sub-chemocline cores (3.5 cm in
860 MUC04 and 9.5 cm in MUC05) are given as numerical values to avoid obscuring the shape of the pore
861 water profile at lower concentrations. Note the differing concentration scales for Mn, Mo and U above
862 and below the chemocline.

Figure 4. Solid phase profiles of Mn/Al, TIC (shaded area), Fe/Al, TS (shaded area), Mo/Al, TOC (shaded area), U/Al and Mo/TOC. Vertical dashed lines represent average Mn/Al, Fe/Al and Mo/Al ratios of the upper continental crust ($(Mn/Al)_{detr}$ = 0.75, $(Fe/Al)_{detr}$ = 0.44, $(Mo/Al)_{detr}$ = 0.19, $(U/Al)_{detr}$ = 0.35; McLennan, 2001). The horizontal arrow between MUC11 and MUC04 indicates the location of the chemocline. Note differing concentration scales for Mn/Al (logarithmic for MUC04 and MUC05), Mo/Al and U/Al above and below the chemocline. Vertical arrows in the Mo/Al diagrams of sub-chemocline cores depict the depth range and mean Mo/Al ratio used for the calculation of $(Mo)_{XS}$ and Mo burial fluxes (see Table 3).

Figure 5. Plot of Mn concentrations versus Ca concentrations for sediments above and below the chemocline.

Figure 6. Plot of Mo_{EF} versus U_{EF} for sediments above and below the chemocline. Note logarithmic scale of both axes. The solid lines depict the mass ratio of Mo/U in seawater (~3.2) times 1.0 and 0.3. The dashed gray lines are adopted from Algeo and Tribovillard (2009) and illustrate (1) increasing sedimentary $(Mo/U)_{XS}$ ratios with decreasing benthic redox potential; (2) sedimentary $(Mo/U)_{XS}$ ratios > seawater related to accelerated Mo accumulation associated with a Mn and Fe shuttle; (3) sedimentary $(Mo/U)_{XS}$ ratios < seawater related to Mo depletion in the water column of permanently euxinic basins. The shaded area depicts the range of $(Mo/U)_{XS}$ ratios of sediment on the Peruvian continental shelf (data from Scholz et al., 2011).

Figure 7. Plot of molar Mo/U ratios in pore water and sediment versus water depth. Note logarithmic scale of x-axis. The vertical dashed line depicts the molar ratio of Mo/U in seawater (~7.5).

Figure 8. Model for accelerated Mo accumulation associated with a Mn and Fe shuttle in (A) a weakly restricted basin with a short deep water residence time or regular inflow events (cf. Algeo and Tribovillard, 2009) and (B) at a euxinic continental margin in the Proterozoic (cf. Poulton and Canfield,

886 2011). Abbreviations are as follows: [ ] = dissolved species in the water column or pore water; Mo-
887 MnFeOx = Mo absorbed to Mn and Fe (oxyhydr)oxides ($MoO_xS_{4-x}^{2-}$, $1 < x < 4$); $MnCO_3$ = Mn carbonates;
888 FeS_X = Fe sulfides; Mo-S-OM = Mo associated with sulfur and organic matter. Note that scavenging of Mo
889 by organic matter or Fe sulfides in the water column is likely to occur in both (A) and (B).

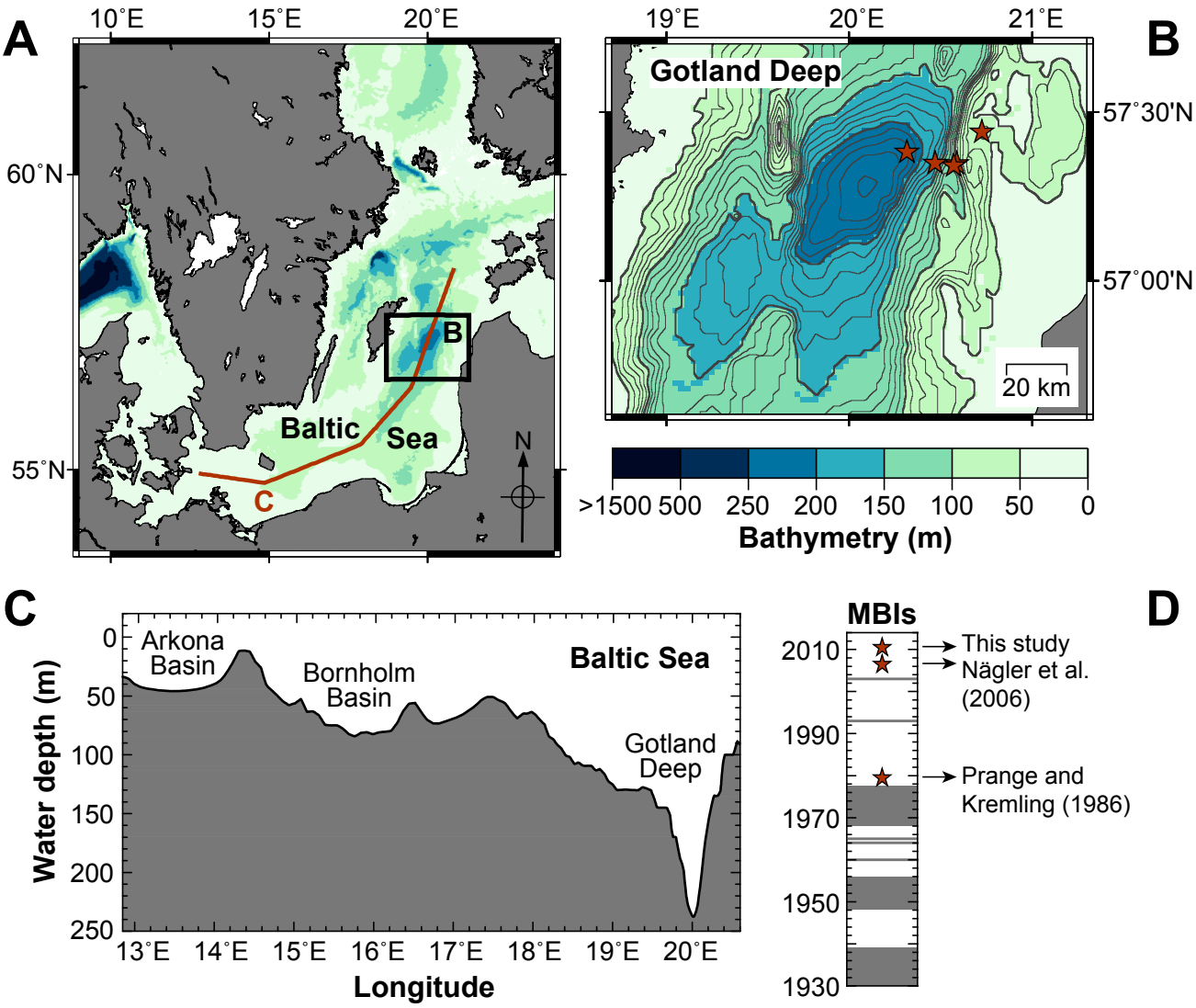
A
10˚E
15˚E
20˚E
60˚N
55˚N
B
C
Baltic
Sea
N
B
19˚E
20˚E
21˚E
Gotland Deep
57˚30'N
57˚00'N
20 km
>1500 500 250 200 150 100 50 0
Bathymetry (m)
C
Water depth (m)
0
50
100
150
200
250
Arkona
Basin
Bornholm
Basin
Baltic Sea
Gotland
Deep
13˚E 14˚E 15˚E 16˚E 17˚E 18˚E 19˚E 20˚E
Longitude
D
MBIs
2010
1990
1970
1950
1930
This study
Nägler et al.
(2006)
Prange and
Kremling (1986)

Figure 1

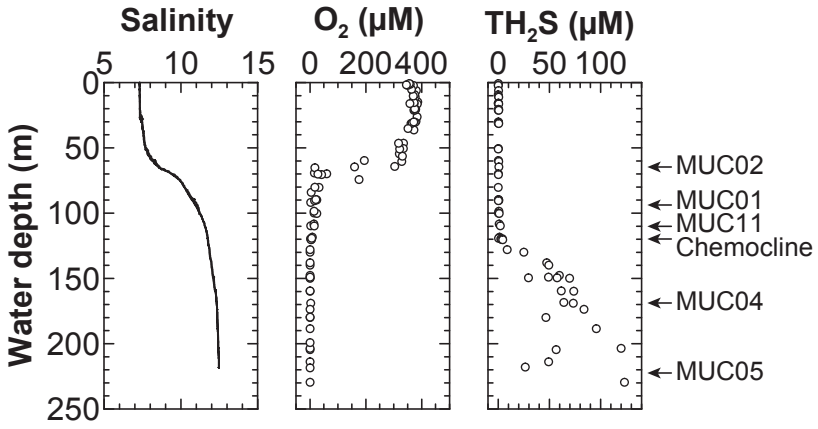
Salinity
O2 (µM)
TH2S (µM)
5 10 15
0 200400
0 50 100
Water depth (m)
0
50
100
150
200
250
MUC02
MUC01
MUC11
Chemocline
MUC04
MUC05

Figure 2

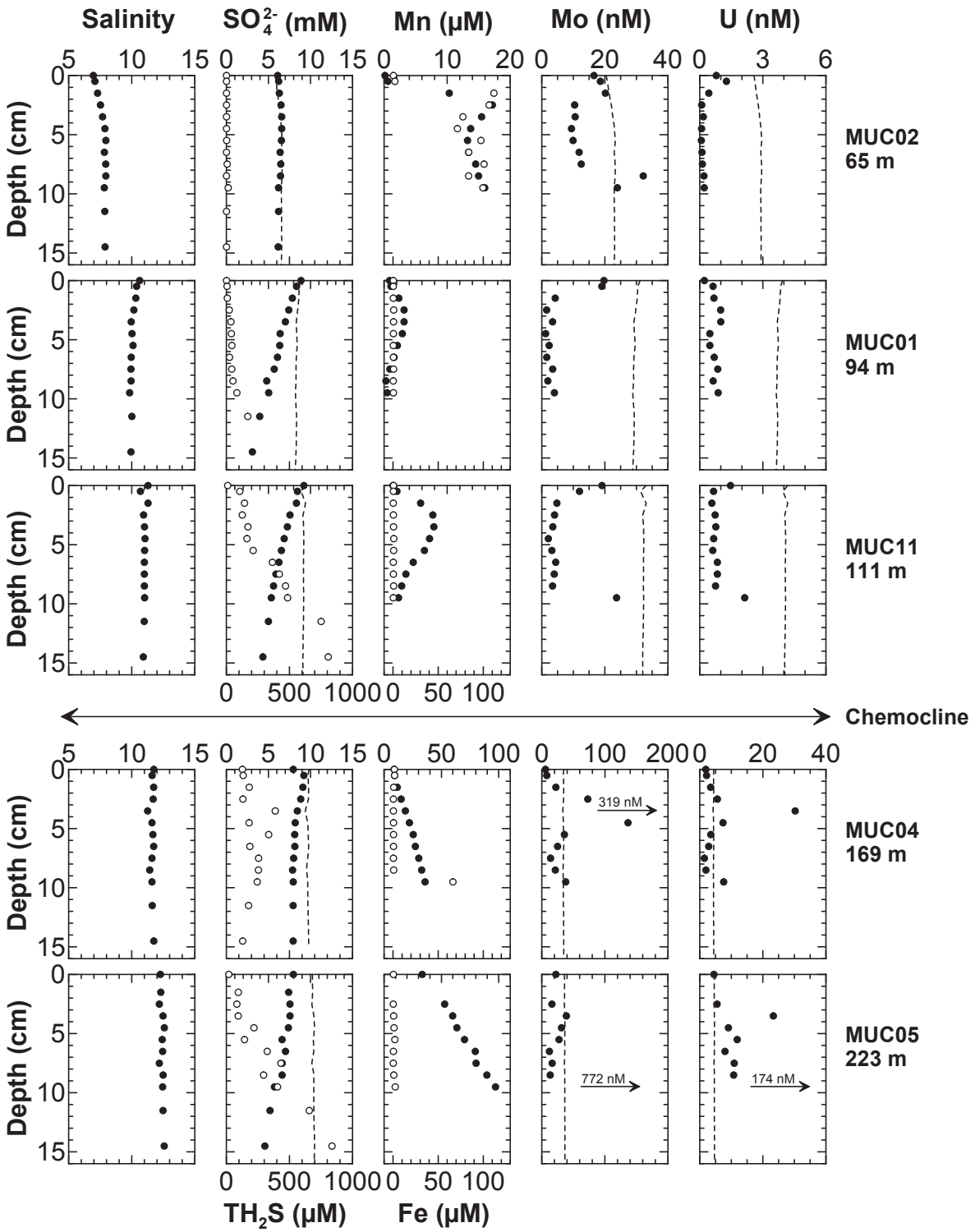
Salinity
SO_4^{2-} (mM)
Mn (μM)
Mo (nM)
U (nM)
Depth (cm)
MUC02
65 m
MUC01
94 m
MUC11
111 m
Chemocline
MUC04
169 m
MUC05
223 m
319 nM
772 nM
174 nM
TH_2S (μM)
Fe (μM)

Figure 3

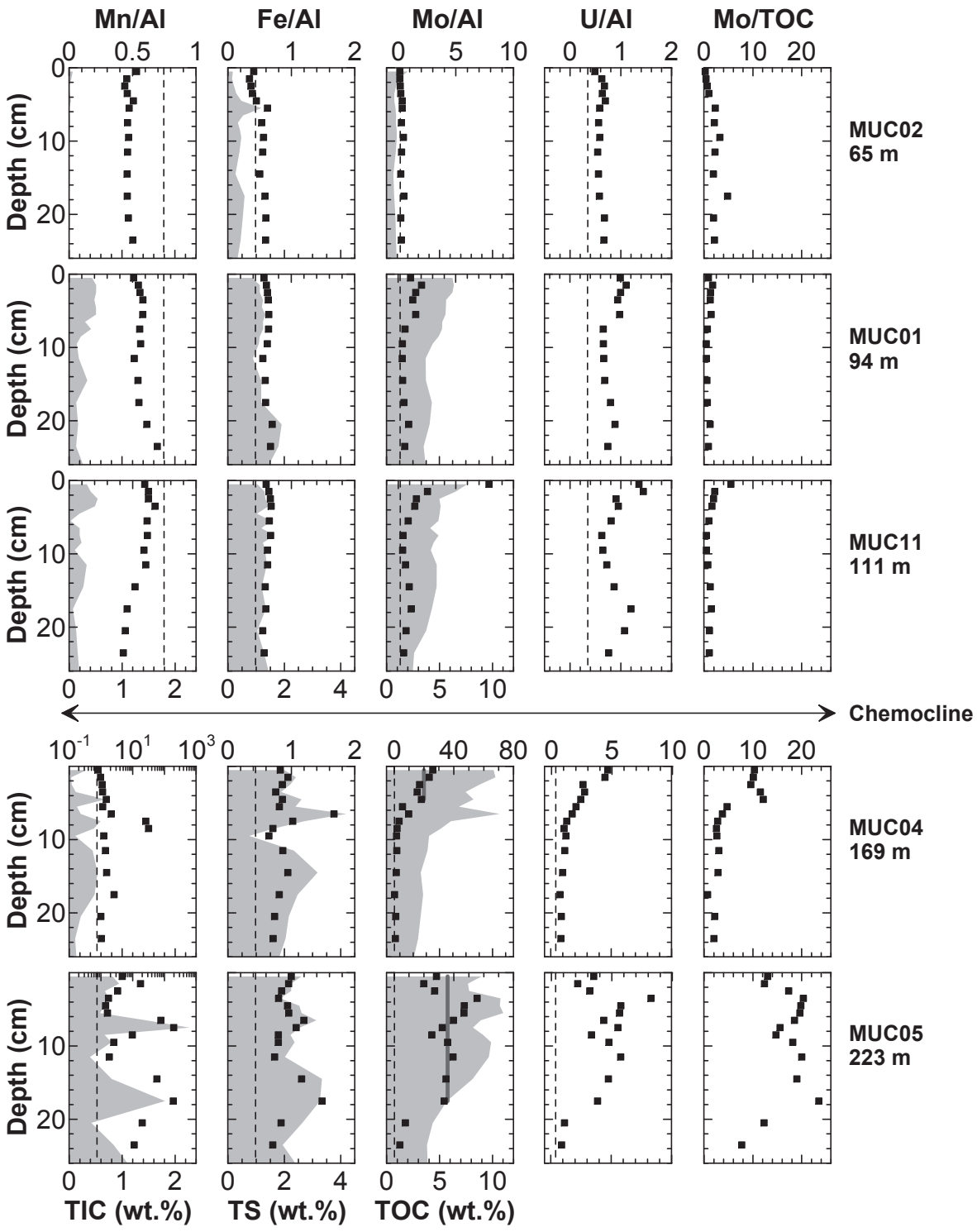
Mn/Al
Fe/Al
Mo/Al
U/Al
Mo/TOC
Depth (cm)
MUC02
65 m
MUC01
94 m
MUC11
111 m
Chemocline
MUC04
169 m
MUC05
223 m
TIC (wt.%)
TS (wt.%)
TOC (wt.%)

Figure 4

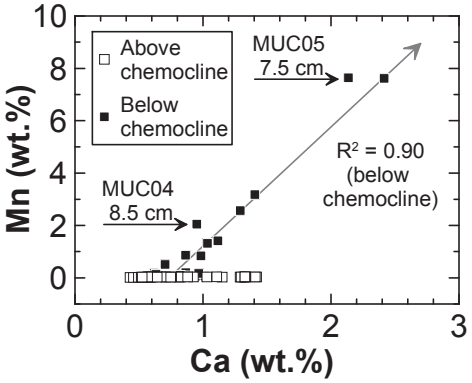
Above chemocline
Below chemocline
MUC05
7.5 cm
MUC04
8.5 cm
R² = 0.90
(below
chemocline)
Mn (wt.%)
Ca (wt.%)
0
2
4
6
8
10
0
1
2
3

Figure 5

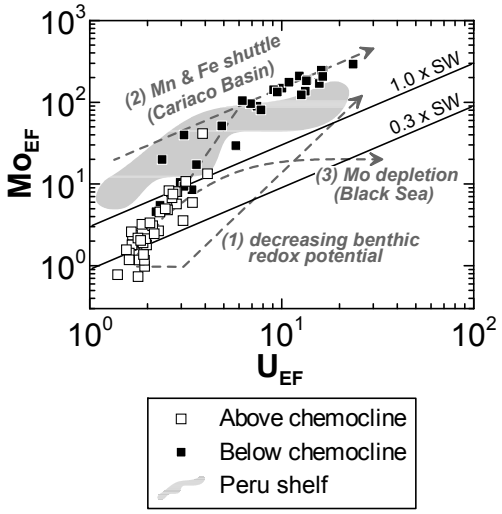
10^3
10^2
10^1
10^0
Mo_{EF}
10^0
10^1
10^2
U_{EF}
(2) Mn & Fe shuttle (Cariaco Basin)
1.0 x SW
0.3 x SW
(3) Mo depletion (Black Sea)
(1) decreasing benthic redox potential
Above chemocline
Below chemocline
Peru shelf

Figure 6

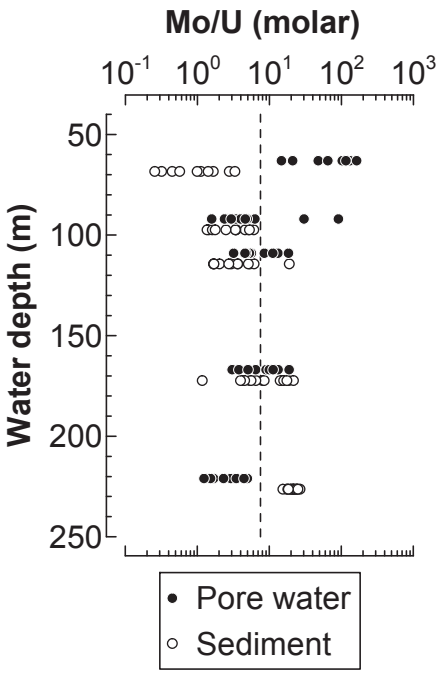
Mo/U (molar)
10-1
100
101
102
103
Water depth (m)
50
100
150
200
250
Pore water
Sediment

Figure 7

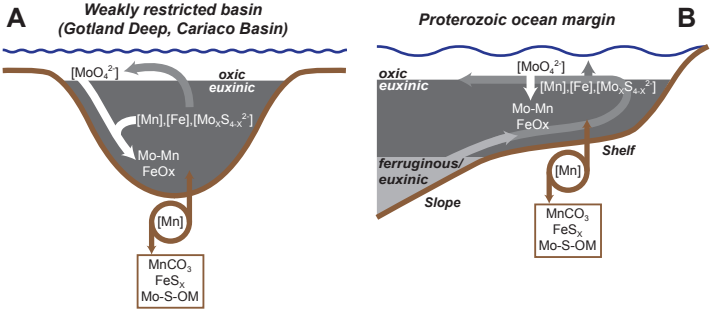
A
Weakly restricted basin
(Gotland Deep, Cariaco Basin)
[MoO4 2-]
oxic
euxinic
[Mn],[Fe],[MoxS4-x 2-]
Mo-Mn
FeOx
[Mn]
MnCO3
FeSx
Mo-S-OM
Proterozoic ocean margin
B
[MoO4 2-]
oxic
euxinic
[Mn],[Fe],[MoxS4-x 2-]
Mo-Mn
FeOx
Shelf
ferruginous/
euxinic
Slope
[Mn]
MnCO3
FeSx
Mo-S-OM

Figure 8

Table 1

Click here to download Table: CHEMGE7114_Table1.xlsx

Table 1. Geographical coordinates and water depth of the sampling stations.
The stations are ordered according to increasing water depth and decreasing bottom water redox potential.

Station AL355	Gear	No.	Latitude N	Longitude E	Water depth
Bottom water $O_2 > 0$ µM, $H_2S = 0$ µM:					
311	MUC	02	57°26.49´	20°43.49´	65
Bottom water $O_2 = 0$ µM, $H_2S = 0$ µM:					
308	MUC	01	57°20.88´	20°35.25´	94
366	MUC	11	57°20.52´	20°34.22´	111
Bottom water $O_2 = 0$ µM, $H_2S > 0$ µM:					
330	MUC	04	57°21.00´	20°28.13´	169
345	MUC	05	57°22.99´	20°18.98´	223

Table 2

Click here to download Table: CHEMGE7114_Table2.xlsx

Table 2. Accuracy of the digestion protocol. Measured values are given as mean ± SD.

	SDO-1[a]		PACS-2[b]		RR9702A-42MC[c]	
	This study (n = 8)	Certified	This study (n = 5)	Certified	This study (n = 13)	Previous studies
Al (wt.%)	6.24 ± 0.12	6.49 ± 0.12	6.32 ± 0.14	6.62 ± 0.32	8.24 ± 0.22	8.40 ± 0.20
Ca (wt.%)	0.74 ± 0.02	0.75 ± 0.03	1.99 ± 0.04	1.96 ± 0.18	2.69 ± 0.07	2.66 ± 0.04
Mn (µg g^{-1})	304 ± 8	325 ± 39	437 ± 9	440 ± 19	527 ± 14	530 ± 15
Fe (wt.%)	6.46 ± 0.14	6.53 ± 0.15	4.16 ± 0.10	4.09 ± 0.06	4.83 ± 0.13	4.80 ± 0.10
Mo (µg g^{-1}), ICP-MS	153 ± 4	134 ± 21	5.46 ± 0.13	5.43 ± 0.28	1.74 ± 0.09	1.90 ± 0.30
Mo (µg g^{-1}), ID ICP-MS	152 ± 4	134 ± 21	5.61 ± 0.14	5.43 ± 0.28	1.81 ± 0.09	1.90 ± 0.30
U (µg g^{-1}), ICP-MS	45.9 ± 1.0	48.5 ± 6.5	2.38 ± 0.04	3[d]	3.09 ± 0.14	3.3 ± 0.15

[a]Devonian Ohio Shale, USGS (Govindaraju, 1994).

[b]Marine Sediment (National Research Council, Canada).

[c]In-house standard, Chilean margin sediment, n > 100 (Muratli et al., 2012).

[d]Information value only.

Table 3

Click here to download Table: CHEMGE7114_Table3.xlsx

Table 3. Parameters and properties used for mass balance calculations.

The basin geometry was computed from bathymetric data (Seifert et al., 2001) by the aid of the Generic Mapping Tool (GMT).

Parameter	Value
150-200 m water depth	
Seafloor area (m^2)	$3.61 \cdot 10^9$
$(Mo)_{conserv}$ (nM)[a]	41.6
$F(Mo)_{xs,burial}$ (nmol m^{-2} yr^{-1})[b]	$1.27 \cdot 10^5$
Below 200 m water depth	
Seafloor area (m^2)	$9.92 \cdot 10^8$
$F(Mo)_{xs,burial}$ (nmol m^{-2} yr^{-1})[c]	$2.14 \cdot 10^5$
Average thickness of water column , z (m)	18
$(Mo)_{conserv}$ (nM)[a]	41.6
Whole basin (defined by 150 m isobath)	
Seafloor area (m^2)	$4.60 \cdot 10^9$
$F(Mo)_{xs,burial}$ (nmol m^{-2} yr^{-1})	$1.47 \cdot 10^5$
Average thickness of anoxic water column, z (m)	90
$(Mo)_{conserv}$ (nM)[a]	41.6
$\tau_{salinity}$ (yr)[d]	20

[a]Conservative Mo concentration based on typical salinity after inflow events (Matthäus et al., 2008).

[b]Caclulated from the mean $(Mo)_{XS}$ above 5 cm sediment depth of MUC04 (169 m water depth) and the mean MAR in the Gotland Deep (Hille et al., 2006).

[c]Calulated from mean $(Mo)_{XS}$ above 19 cm sediment depth of MUC05 (223 m water depth) and the mean MAR in the Gotland Deep.

[d]Reissmann et al. (2009).

Electronic Supplement Table 1

Click here to download Table: CHEMGE7114_Electronic Supplement_Table 1.xlsx

Electronic Supplement Table 1. Bottom water (BW) and pore water data.

Station AL355-No.	Gear	No.	Depth, squeezer (cm)	Cl^- (mM)	SO_4^{2-} (mM)	TH_2S (µM)	Depth, rhizons (cm)	Mn^a (µM)	Fe^b (µM)	Mo (nM)	U (nM)
310	MUC	2	BW	111	6.11	1.1	BW	0.16	0.36	16.6	0.79
			0-1	113	6.22	1.3	0.5	0.61	1.83	18.6	1.27
			1-2	117	6.30	1.3	1.5	10.32	111.95	20.2	0.42
			2-3	120	6.51	1.3	2.5	17.17	106.57	10.4	0.09
			3-4	123	6.57	1.7	3.5	15.45	77.58	10.6	0.16
			4-5	126	6.57	1.4	4.5	13.72	71.32	9.4	0.09
			5-6	127	6.54	2.6	5.5	13.23	97.39	9.9	0.08
			6-7	125	6.40	1.2	6.5	13.40	84.02	11.8	0.10
			7-8	127	6.47	6.2	7.5	14.52	100.97	12.5	0.12
			8-9	127	6.43	1.2	8.5	14.98	83.82	32.2	0.20
			9-10	125	6.21	14.8	9.5	15.95	99.81	23.9	0.21
			10-13	126	6.21	1.3					
			13-16	126	6.16	1.1					
			16-19	125	6.03	1.1					
			19-22	124	5.58	1.3					
			22-25	123	5.46	1.1					
			25-28	123	5.52	1.1					
307	MUC	1	BW	170	8.86	1.5	BW	0.88	0.19	19.7	0.22
			0-1	166	8.34	4.5	0.5	1.08	0.21	19.1	0.63
			1-2	165	7.84	7.9	1.5	2.34	0.19	4.3	0.68
			2-3	163	7.43	22.5	2.5	3.18	0.64	1.6	0.99
			3-4	159	7.02	36.7	3.5	3.18	0.44	3.4	1.00
			4-5	160	6.39	40.6	4.5	2.89	0.40	1.2	0.48
			5-6	162	6.34	43.6	5.5	2.11	0.21	2.4	0.48
			6-7	159	6.07	24.7	6.5	1.57	0.37	1.6	0.68
			7-8	159	5.67	42.5	7.5	0.93	0.55	3.4	0.86
			8-9	159	4.81	53.0	8.5	0.30	0.15	1.9	0.64
			9-10	157	5.02	83.9	9.5	0.48	0.33	4.0	0.87
			10-13	160	3.97	171					
			13-16	159	3.09						
			16-19	155	2.40	197					
			19-22	158	1.90	233					
			22-25	154	1.51	178					
			25-28	155	1.36	223					
365	MUC	11	BW	181	9.22	10	BW	1.42	0.47	19.1	1.46
			0-1	171	8.46	106	0.5	2.05	0.28	11.9	0.65
			1-2	181	8.33	143	1.5	5.79	0.21	4.8	0.57

Electronic Supplement Table 2

Click here to download Table: CHEMGE7114_Electronic Supplement_Table 2.xlsx

Electronic Supplement Table 2. Solid phase data.

Station AL355-No.	Gear	No.	Depth (cm)	TOC (wt.%)	TS (wt.%)	TIC (wt.%)	Al (wt.%)	Ca (wt.%)	Mn (wt.%)	Fe (wt.%)	Mo ($\mu g\ g^{-1}$)	U ($\mu g\ g^{-1}$)
311	MUC	2	0-1	1.98	0.17	0.07	3.20	0.59	0.02	1.30	0.47	1.56
			1-2	1.12	0.15	0.04	3.21	0.50	0.01	1.09	0.45	2.01
			2-3	0.91	0.21	0.00	3.10	0.43	0.01	1.12	0.58	2.10
			3-4	0.73	0.29	0.01	3.23	0.46	0.01	1.24	0.72	2.04
			4-5	0.72	0.48	0.04	3.82	0.50	0.02	1.71	1.31	2.65
			5-6	0.84	1.19	0.00	5.65	0.54	0.03	3.51	1.94	3.28
			6-7	0.91	0.54	0.02						
			7-8	0.88	0.35	0.02	6.80	0.60	0.03	3.61	1.85	3.82
			8-9	0.95	0.43	0.01						
			9-10	0.96	0.47	0.00	6.86	0.58	0.03	3.84	3.11	4.01
			10-13	0.86	0.40	0.00	6.52	0.57	0.03	3.57	1.95	3.54
			13-16	0.63	0.27	0.01	5.40	0.52	0.02	2.72	1.22	3.03
			16-19	0.71	0.59	0.01	6.85	0.59	0.03	3.98	3.39	3.95
			19-22	0.84	0.52	0.02	7.35	0.57	0.03	4.39	1.62	4.96
			22-25	0.88	0.45	0.00	7.27	0.57	0.04	4.30	1.89	4.84
			25-28	0.94	0.32	0.01						
308	MUC	1	0-1	6.23	0.85	0.44	5.12	1.32	0.03	2.91	5.55	5.07
			1-2	6.36	1.13	0.51	5.49	1.29	0.03	3.33	11.23	6.07
			2-3	6.24	1.13	0.51	5.47	1.30	0.03	3.42	8.40	5.45
			3-4	5.64	1.24	0.48	5.51	1.42	0.03	3.51	7.09	5.17
			4-5	5.62	1.21	0.51						
			5-6	5.57	1.32	0.51	5.31	1.41	0.03	3.42	8.14	5.19
			6-7	5.28	1.24	0.30						
			7-8	5.25	1.25	0.41	5.72	1.33	0.03	3.67	3.50	3.75
			8-9	4.93	1.13	0.22						
			9-10	4.37	1.10	0.14	5.48	1.03	0.03	3.42	2.02	3.61
			10-13	3.71	0.88	0.19	5.12	0.82	0.03	2.83	1.85	3.40
			13-16	3.73	1.18	0.35	5.43	1.15	0.03	3.21	2.21	3.72
			16-19	4.29	1.18	0.14	5.64	0.74	0.03	3.35	2.87	4.51
			19-22	4.09	1.90	0.17	5.46	0.67	0.03	3.82	5.02	4.85
			22-25	3.52	1.79	0.13	5.32	0.92	0.04	3.58	3.13	3.97
			25-28	3.72	1.38	0.29						
366	MUC	11	0-1	7.61	1.05	0.33	5.30	1.33	0.03	3.20	41.71	7.19
			1-2	6.54	1.30	0.41	5.62	1.33	0.04	3.62	14.26	8.09
			2-3	4.99	1.33	0.54	6.18	1.33	0.04	4.13	9.72	5.60
			3-4	5.09	1.44	0.49	5.84	1.11	0.04	3.96	8.35	5.55
			4-5	5.01	1.03	0.20						